Contrasting patterns of change in snowline altitude across five Himalayan catchments

Orie Sasaki[1], Evan S. Miles[2], Francesca Pellicciotti[2], Akiko Sakai[1], Koji Fujita[1]

[1]Graduate School of Environmental Studies, Nagoya University, Nagoya, 484－8601, Japan
[2]Swiss Federal Institute for Forest, Snow, and Landscape Research WSL, Birmensdorf, CH-8903, Switzerland

Correspondence to: Orie Sasaki (Sasaki.o.ab@m.titech.ac.jp)

Abstract.

Seasonal snowmelt in the high~~ mountain~~ mountains of Asia is an important source of river discharge. ~~Observing the spatial and temporal variation of~~Therefore, observation of the spatiotemporal variations in snow cover at catchment scales using high-resolution satellites is essential ~~to~~for understanding ~~the~~ changes in water supply from headwater catchments. In this study, we ~~propose~~adapt an algorithm to automatically detect the snowline altitude (SLA) using the Google Earth Engine platform with available high-resolution multispectral satellite archives~~, which~~ that can be readily applied ~~globally.~~for areas of interest. Here, we ~~apply~~applied and ~~evaluate~~evaluated the tool to five glacierised watersheds across the Himalayas to quantify the changes in seasonal and annual snow cover over the past 21 years~~,~~ and analyse climate reanalysis data to ~~analyze~~assess the meteorological factors influencing the SLA. Our findings ~~reveal~~revealed substantial variations in the SLA among ~~the~~ sites in terms of seasonal patterns, decadal trends, and meteorological controls. We identify positive trends in SLA ~~has been increasing in~~in the Hidden Valley (+11.9 m yr^{-1}), Langtang Valley (+14.4 m yr^{-1}), and Rolwaling Valley (+8.2 m yr^{-1}) in the Nepalese Himalaya, but ~~decreasing in~~a negative trend at Satopanth ~~(~~(−15.6 m yr^{-1}) in the western Indian Himalaya, ~~while we find~~ and no significant trend in Parlung Valley in southeast Tibet. We suggest that the ~~increasing~~increase in SLA ~~is~~in Nepal was caused by warmer temperatures during the monsoon ~~in Nepal~~season, whereas ~~decreases~~the decrease in SLA ~~are~~in India was driven by increased winter snowfall and reduced monsoon snowmelt~~ in India~~. By integrating the outcomes of these analyses, we ~~find~~found that long-term changes in SLA are primarily driven by shifts in the local climate, ~~while~~whereas seasonal variability may be influenced by geographic features in conjunction with climate.

Style Definition: Normal
Style Definition: Heading 5
Style Definition: Heading 6
Style Definition: Title
Style Definition: Subtitle

Formatted: Superscript
Formatted: Superscript
Formatted: Superscript
Formatted: Font: Gungsuh
Formatted: Font: Gungsuh
Formatted: Font: Gungsuh
Formatted: Superscript

1 Introduction ~~(as Heading 1)~~

Snow is an essential water resource in the high ~~mountain~~mountains of Asia (HMA~~)~~), as it supplies ~~meltwater~~melted water to downstream regions and regulates seasonal streamflow, especially ~~in~~during drought years (Pritchard, 2019; Kraaijenbrink et al., 2021). ~~This mountain~~Mountain-sourced water ~~supply~~supplies are increasingly ~~sustains~~sustaining human society through ~~water for~~ drinking, irrigation, industrial, and hydropower generation (Immerzeel et al., 2020; Viviroli et al., 2020). Snow has a cooling effect on the atmosphere~~,~~ by reflecting shortwave radiation and maintaining freezing ground temperatures, and ~~decreasing snow~~ decrease in the extent of snow has been suggested as one of the causes of high-elevation warming (~~e.g.,~~ Palazzi et al., 2019). ~~Knowledge of~~Therefore, understanding the current and past snow cover distribution, its ongoing changes, and its driving factors are fundamentally important.

Several studies have addressed ~~the~~ variations ~~of~~in snow cover in detail for individual watersheds (e.g., Gironoa-Mata et al., 2019; Stigter et al., 2017), ~~while~~whereas large-scale assessments have predominantly focused on annual values with moderate~~-~~-resolution sensors (> 500 m) such as MODIS (Smith et al., 2018; ~~Lievens et al., 2019;~~ Tang et al., 2020; Kraaijenbrink et al., 2021). ~~Analysis~~Past studies have used MODIS to provide a strong baseline understanding of ~~seasonal variation in~~ global and regional snow phenology, including snow cover ~~provides more detailed information than annual values about the snow dynamics and their relationship with climatic~~duration and ~~geographic factors (Girona-Mata~~extent (e.g. Johnston et al., 2023; Notarnicola, 2022; Roessler & Dietz, 2023). MODIS snow products have been essential for the constraint of snow reanalyses (Kraaijenbrink et al., ~~2019). While~~2021; Liu et al., 2021), but standard MODIS snow products may overestimate snow cover in HMA and require additional processing (Muhammad & Thapa, 2020). Furthermore, although MODIS provides a daily temporal resolution and a broad perspective, but the coarse spatial resolution of retrievals (~~500m~~500 m) poorly resolves topographic features~~, leading to the use of~~; fractional snow~~-~~ cover products ~~(e.g.,~~are a key advance but do not mitigate this problem (Painter et al., 2009; Rittger et al, 2021). Because catchment-scale snow cover derived from MODIS can be affected by cloud cover ~~due~~owing to spectral similarities ~~of~~between clouds and snow (Stillinger et al, 2019), it can be biased by high-elevation snow-free areas and ~~struggles~~struggle with shadows and subpixel effects in the extreme high-relief topography of the Himalayas (~~e.g.,~~ Girona-Mata et al., 2019).

The snowline altitude (SLA) is a useful metric to study snow cover variations at annual and seasonal time scales since it integrates both snowfall and snowmelt dynamics and is independent of catchment hypsometry (Girona-Mata et al., 2019; Deng et al., 2021). SLA is less biased by cloud cover than snow cover extent and is useful for evaluating and constraining hydrological models (e.g., Krajčí et al., 2014~~).~~, Buri~~On glaciers, it can also be used as a proxy for the equilibrium line altitude (e.g., Spiess~~ et al~~, 2016; Racoviteanu~~., 2023, 2024, Robinson et al., ~~2019~~2025). The seasonal pattern and aspect dependency of SLA are particularly useful to reveal the primary controls of snow cover dynamics (e.g., Girona-Mata et al., 2019). On glaciers, it can also be used as a proxy for the equilibrium line altitude (e.g., Spiess et al, 2016; Racoviteanu et al., 2019) and to constrain glacier mass balance (e.g. Mernild et al., 2013; Barandun et al, 2018). By reflecting the interplay between solid precipitation and melt, changes in seasonal snowlines can provide an important and simple indicator of climatic changes. Several previous studies have derived SLA and its changes on various scales; e.g., individual catchments to continental scales (e.g., McFadden et al., 2011; Racoviteanu et al., 2019; Girona-Mata et al., 2019; ~~Tange~~Tang et al., 2020). In High Mountain Asia, most studies have used MODIS to examine SLA changes, and have highlighted a broad tendency towards shorter snowcover periods excepting the western Himalaya, part of eastern Tibet, and part of the eastern Tien Shan (Tang et al., 2022). However, none of them have examined SLA changes and the primary controls of SLA variations at high resolution and in multiple regions, to identify and understand regional differences.

Analysis of seasonal variations in snow cover at high spatial resolution provides insights into snow dynamics and their relationships with climatic and geographic factors (Girona-Mata et al., 2019).

~~The knowledge~~Knowledge of the regional variation ~~of~~in the SLA, its seasonal controls, and ~~its sensitivity to climatic and geographic factors could provide~~ ongoing changes provides an important basis for a deeper understanding of ~~past to~~current and future changes in snow cover under climate change. ~~Hence, this~~This study ~~aims~~therefore aimed to ~~investigate~~answer the following research questions: 1. How does snowline seasonality vary across the ~~climatic gradient of the~~ Himalayas? 2. ~~Do the~~ Which meteorological factors play a dominant role in controlling ~~factors also vary? 3.~~ SLA throughout the year across this region? 3. How much ~~have snowlines shifted (~~and in which months~~) over~~ has the ~~past 20 years?~~

~~2 Study site and data~~

~~2.1 Study sites~~

~~We selected five glacierized catchments along the Himalayas (Fig. 1), where hydro-glaciological studies and glacier monitoring programs have been conducted in recent years. The catchments, which we identify after the representative glacier, river, or valley, are, from west to east, Satopanth, Hidden Valley, Langtang Valley, Rolwaling Valley, and Parlung (Fig. 1). The catchments have mean elevations ranging from 3,864 m to 5,384 m, and include numerous glaciers covering 6.8% to 38.7% of the~~ snowline shifted in the recent 21st-century? 4. Which climatic changes are associated with these changes in catchment ~~area (Table 1). Although the Asian summer monsoon dominates the climate of the entire range, the monsoon intensity varies considerably across the five catchments. Satopanth Catchment receives limited summer precipitation and moderate winter snow from westerly disturbances (Cannon et al., 2015; Bao et al., 2019), while Parlung experiences considerable spring precipitation (Yang et al., 2013). In the other three regions, most of the annual precipitation occurs from June to September (Fig. S1).~~

g

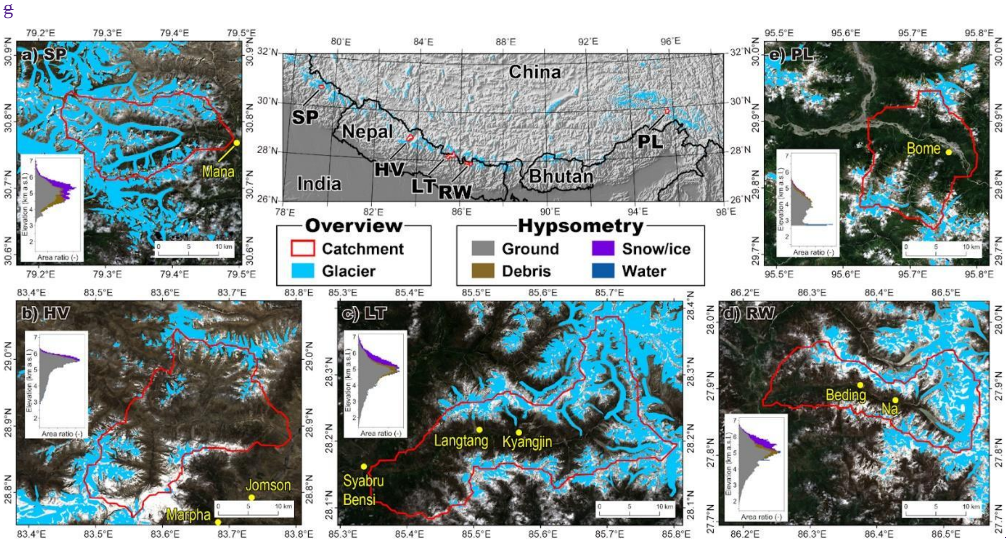

~~Figure 1: Upper center figure shows the location of target catchments (from west to east; Satopanth (SP), Hidden Valley (HV), Langtang Valley (LT), Rolwaling Valley (RW), Parlung (PL)). Enlarged views of target catchments are shown in surrounding figures; (a) Satopanth (SP), (b) Hidden Valley (HV), (c) Langtang Valley (LT), (d) Rolwaling Valley (RW), and (e) Parlung (PL). Catchment outlines~~

and glaciers are indicated by red and light blue polygons, which are sourced from HydroSHEDS (Lehner and Grill, 2013) and GAMDAM (Sakai, 2019) databases, respectively. Yellow dots denote representative villages. The background images of (a)-(e) are composite images created using the Sentinel-2 images acquired between 2017 to 2020.

Table 2: Information on target catchments

	Central coordinate	Median altitude [m a.s.l.] (Max; Min)	Area [km^2]	Glacierised area [km^2]	Annual total precip. [mm]	Daily mean air temp. [°C]
Satopanth	79.36°E, 30.78°N	5,031 (7,080; 3,154)	243.0	94.0 (39 %)	1,654	−7.5
Hidden Valley	83.63°E, 28.91°N	5,384 (6,492; 2,876)	445.0	49.1 (11 %)	801	−8.4
Langtang	85.58°E, 28.21°N	4,879 (7,156; 1,461)	587.7	144.6 (25 %)	1,978	−3.7
Rolwaling	86.41°E, 27.89°N	5,008 (6,897; 1,621)	309.5	76.8 (25 %)	1,170	−3.9
Purlung	95.71°E, 29.84°N	3,864 (6,052; 2,678)	253.2	17.1 (7%)	2,056	−2.2

2.2 Data

To determine the boundaries of the target catchment, we used HydroBASINS version 1.0 from the HydroSHEDS database (Lehner and Grill, 2013). HydroBASINS provides 12 levels of nested watershed boundaries according to their stream order, from which we chose Level 9 for the target catchments comparable in size to that used in Girona-Mata et al. (2019).

We used Level-1 top-of-atmosphere (TOA) reflectances for Landsat 5/7/8 data and Level-1C TOA reflectance for Sentinel-2 to detect the snow-covered area (see Method). The spatial resolutions of these datasets are 30 m for Landsat 5/7/8, 10 m for visible bands of Sentinel-2, and 20 m for SWIR bands of Sentinel-2. To select scenes, we identified all scenes in the 1999-2019 period whose internal metadata indicated a cloud cover less than 50% of the scene. This resulted in a total of 6,128 scenes; 1,384 for Satopanth, 1,173 for Hidden Valley, 967 for Langtang, 1,520 for Rolwaling, and 1,084 for Parlung.

Our method requires a reference digital surface elevation model (DEM); for this, we used the ALOS World 3D—30m (AW3D30) version 2.2 which was produced from measurements by the Panchromatic Remote-sensing Instrument for Stereo Mapping (PRISM) on board the Advanced Land Observing Satellite (ALOS). The spatial resolution of AW3D30 is approximately 30 m (1-arcsecond mesh). The target accuracy of AW3D30 is set to 5 m (root mean square value) both vertically and horizontally (Takaku and Tadono, 2017).

We used three kinds of land surface classification data; glacier outlines from the latest version of the GAMDAM inventory (Nuimura et al., 2015; Sakai, 2019), outlines of supraglacial debris detected by Scherler et al. (2018), and maps of surface water bodies named "Global Surface Water" created by the Joint Research Center (Pekel et al., 2016). These data sets were used to determine the catchment surface types and mask areas that may be erroneously identified as snow, such as glaciers and water surfaces.

~~High-resolution multi-spectral imageries from RapidEye and PlanetScope were employed to validate the automatically detected snowline altitude by manual delineation. RapidEye and PlanetScope are both Earth observation constellations operated by Planet Labs, with spatial resolutions of 6.5 m and 3.7 m. We prepared one to three ortho-images for each target catchment which are obtained close to the date the automatic detections are conducted from Landsat 5/7/8 or Sentinel-2 images. The list of used images is shown in Table 2.~~

~~We obtained 0.25° gridded near-surface 2m air temperature, downward surface shortwave radiation, and precipitation from ERA5 (Hersbach et al., 2020). We aggregated the hourly product to daily and monthly mean datasets. The air temperature was corrected to the average~~ snowline ~~altitude during the target period (1999 to 2019) in each catchment using a standard environmental lapse rate (0.065 °C m-1).~~?

Formatted: Indent: First line: 0.14"

~~3 Method~~

2 Methods

~~3.1. Detection of snowline altitude~~

Our method to delineate snowline altitudes closely follows that of Girona-Mata et al. (2019) but is implemented in Google Earth Engine. ~~In our detection tool, by inputting the latitude and longitude of a certain point, the catchment area containing the point is automatically selected from the HydroSHEDS database. Satellite images covering the catchment are then collected from Landsat 5/7/8 and Sentinel-2 with the criterion of less than 50% cloud cover. An average of about 1,200 satellite images are collected for one catchment area over the past 21 years in this study~~A schematic diagram of the method is shown in Figure 1. The framework uses an automated processing to map snowcover, masking confounding landcover types, identify boundaries of the snowcovered area, and finally retrieve topographical information corresponding to the SLA. Here we explain the approach and input datasets in more detail, before introducing our test sites and the data evaluation and analysis.

2.1. Detection of snowline altitude

Our method starts with the identification of a catchment of interest, specified by Latitude and Longitude. Based on these coordinates, we automatically determine the boundaries of the target catchment from the HydroBASINS version 1.0 from the HydroSHEDS database (Lehner and Grill, 2013). HydroBASINS provides 12 hierarchical levels of nested watershed boundaries according to their stream order, from which we chose level 9 for the target catchments, which is comparable in size to that used in Girona-Mata et al. (2019). To refine the domain of investigation, we used three kinds of land surface classification data: (1) glacier outlines from the latest version of the GAMDAM inventory (Nuimura et al., 2015; Sakai, 2019), (2) outlines of supraglacial debris detected by Scherler et al. (2018), and (3) maps of surface water bodies named “Global Surface Water” created by the Joint Research Center (Pekel et al., 2016). We used these datasets to mask these surface types, as areas that may be erroneously identified as snow.

Next, the tool collects multispectral data for the target domain. We used Level-1 top-of-atmosphere (TOA) reflectance for Landsat 5/7/8 data and Level-1C TOA reflectance for Sentinel-2 data to detect snow-covered areas. The spatial resolutions of these datasets were 30 m for Landsat 5/7/8, 10 m for the visible bands of Sentinel-2, and 20 m for the SWIR bands of Sentinel-2. We identified all scenes from to 1999–2019 period whose internal metadata indicated a cloud cover of less than 50% of the scene.

To determine the snow-covered area, we calculated the Normalized Difference Snow Index (NDSI; Dozier, 1989) which is defined as the relative magnitude ~~between~~of the reflectance of the visible (green) ~~band~~ and shortwave infrared (SWIR) ~~band (Table 2). We use~~bands. The NDSI approach is an established, robust and accessible method for mapping snow in a variety of illumination and atmospheric conditions, and is applicable to both TOA and surface reflectance values. There is an extensive precedent for NDSI as a practical method for identifying snow, although threshold values are not always transferable between settings (e.g. Burns & Nolin, 2014; Dozier, 1989; Gascoin et al., 2019; Härer et al., 2018). We masked clouds based on the metadata associated with each scene, then used an NDSI threshold of 0.45 ~~following Girona-Mata et al. (2019),~~to identify snow covered areas, which is relatively conservative but ~~performed~~performs well against independent high-resolution measurements and spectral-unmixing approaches (Girona-Mata et al., 2019). Saturation issues are common in Landsat 5/7, where the input signal exceeds the maximum measurable signal~~,~~ and may bias ~~detected snow-covered areas; they have been improved in Landsat 8 and Sentinel-2.~~the detected snow-covered areas. Considerable sensor improvements were made with Landsat 8 and Sentinel-2 in terms of radiometric resolution (mitigating saturation problems, as well as sensor stability, and acquisition schedule, but fortunately, snow and ice can be mapped effectively with established approaches (Paul et al., 2016). Rittger et al. (2021) evaluated the impact of band saturation ~~by~~ using 25 images of Landsat 7 in the Himalayas and reported that 28% of ~~the~~ snow-covered pixels ~~are~~were saturated in the visible bands. ~~We mitigate this~~This problem was mitigated by ~~choosing~~selecting a ~~fairly~~ conservative NDSI threshold (0.45) ~~instead of a marginal threshold (0.4).~~for identifying snow.

Next, we ~~delineate~~delineated the snowline from the derived snow cover map ~~by~~ using ~~a~~the Canny edge detection algorithm (Canny, 1986) which produces ~~smooth~~clean edges ~~in images using a multi-stage process. At~~based on filtered local high values in image gradient. However, at this point, ~~however,~~ the snowline may include misidentified areas because ~~the~~ snow-covered ~~area is~~areas are often obscured by clouds, shadows, scan line corrector (SLC) error stripes, or band saturation over snow. For example, the boundary of ~~the~~an obscured area may be misidentified as a snowline if ~~a cloud covers~~clouds cover the actual boundary of a snow-covered area. ~~We therefore remove~~Therefore, we removed snowlines ~~on the~~from potentially erroneous areas~~:~~ such as cloud cover, deep shadows, SLC-error stripes (Landsat 7), and ice and water surfaces. ~~These~~The last two categories (removal of surface ice and water surfaces) were not implemented in Girona-Mata et al. (2019~~)~~), but the NDSI can return high values for both surfaces, even when snow is not present (i.e., frozen water or bare glacier ice), which could bias the results. As ~~in~~per Girona-Mata et al. (2019), we also ~~remove~~removed very small polygons (smaller than 35 pixels) to eliminate the effects of rock outcrops which may not be relevant to meteorological patterns (i.e., over steepened slopes that cannot hold snow).

~~Subsequently, the~~ Finally, we retrieve topographic information for each point on the snowline boundary, including elevation, slope, and aspect. As a reference digital surface elevation model (DEM), we used the ALOS World 3D－30 m (AW3D30) version 2.2 which was produced from measurements by the Panchromatic Remote-sensing Instrument for Stereo Mapping (PRISM) on board the Advanced Land Observing Satellite (ALOS). The spatial resolution of AW3D30 is approximately 30 m (1-arcsecond mesh). ~~is~~The target accuracy of AW3D30 was set to 5 m (root mean square value) both vertically and horizontally (Takaku and Tadono, 2017).

Finally, we calculated ~~from the DEM to investigate orographic effects. The aspect is classified into four groups; east (45-135°), south (135-225°), west (225-315°), and north (315-360° and 0-45°). Then, we calculate~~ the median snowline altitude for (i) the entire catchment, and (ii) each 45-degree aspect group ~~in~~of each catchment. ~~The above processes are~~ This process was repeated for all available images for each study area.

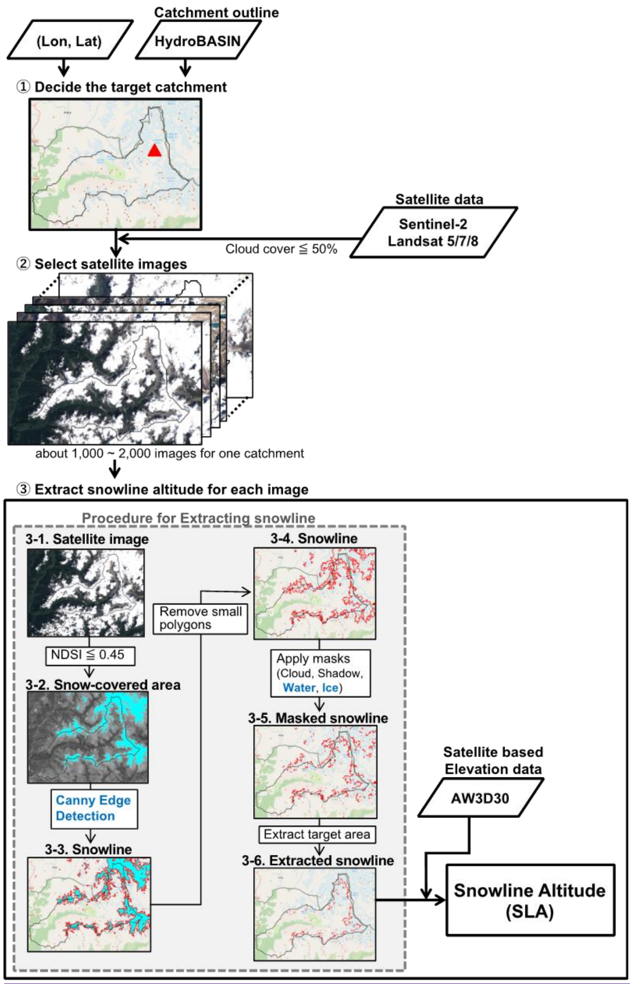

Figure 1. Schematic diagram of the snowline detection algorithm with a sample image obtained from Sentinel-2. The parts highlighted in blue represent updates to the method of Girona-Mata et al. (2019). By inputting longitude and latitude, all procedures are automatically performed on the Google Earth Engine platform.

2.2 Study sites

We selected five glacierised catchments along the Himalayas (Fig. 2), where hydro-glaciological studies and glacier monitoring programs have been conducted in recent years. The catchments that we identified after the representative glacier, river, or valley were, from west to east, Satopanth, Hidden Valley, Langtang, Rolwaling, and Parlung (Fig. 2). The catchments have mean elevations ranging from 3,864 m to 5,384 m and include numerous glaciers covering 6.8% to 38.7% of the catchment area (Table 1). Although the Asian summer monsoon dominates the climate over its entire range, the monsoon intensity varies considerably across the five catchments. The Satopanth receives limited summer precipitation and moderate winter snow from westerly disturbances (Cannon et al., 2015; Bao et al., 2019), whereas the Parlung experiences considerable spring precipitation (Yang et al., 2013). In the other three regions, most annual precipitation occurred from June to September (Fig. S1). Our scene selection criteria for these sites resulted in 6,128 scenes: 1,384 for Satopanth, 1,173 for Hidden Valley, 967 for Langtang, 1,520 for Rolwaling, and 1,084 for Parlung, spread across the 1999-2019 study period (Fig. S3-S7).

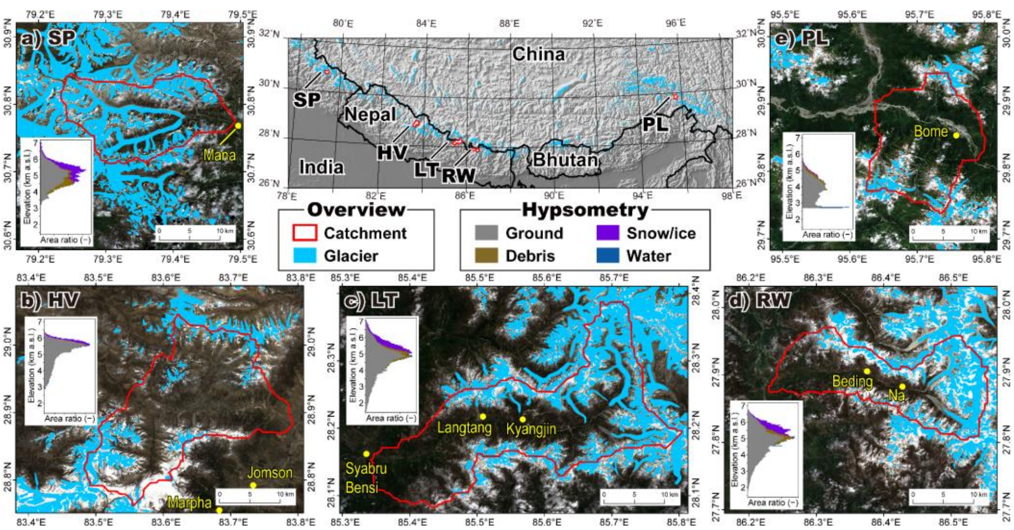

Figure 2: Upper center figure shows the location of target catchments (from west to east; Satopanth (SP), Hidden Valley (HV), Langtang (LT), Rolwaling (RW), Parlung (PL)). Enlarged views of target catchments are shown in surrounding figures; (a) Satopanth (SP), (b) Hidden Valley (HV), (c) Langtang (LT), (d) Rolwaling (RW), and (e) Parlung (PL). Catchment outlines and glaciers are indicated by red and light blue polygons, which are sourced from HydroSHEDS (Lehner and Grill, 2013) and GAMDAM (Sakai, 2019) databases, respectively. Yellow dots denote representative villages. The background images of (a)-(e) are composite images created using the Sentinel-2 images acquired between 2017 to 2020.

~~3.2. Manual delineation for evaluation~~**Table 1: Information on target catchments. Catchment geometric characteristics were derived from the HydroBasins level 9 catchment boundaries and the ALOS World 3D 30m DEM, and glacier geometries from the Randolph Glacier Inventory 6.0, while the climatological characteristics were determined from ERA5, downscaled with an adiabatic lapse rate to the median catchment snowline elevation (see Results).**

	Central coordinate	Median altitude [m a.s.l.] (Max; Min)	Area [km^2]	Glacierised area [km^2]	Annual total precip. [mm]	Daily mean air temp. [°C]
Satopanth	79.36°E, 30.78°N	5,031 (7,080; 3,154)	243.0	94.0 (39 %)	1,654	−7.5
Hidden Valley	83.63°E, 28.91°N	5,384 (6,492; 2,876)	445.0	49.1 (11 %)	801	−8.4
Langtang	85.58°E, 28.21°N	4,879 (7,156; 1,461)	587.7	144.6 (25 %)	1,978	−3.7
Rolwaling	86.41°E, 27.89°N	5,008 (6,897; 1,621)	309.5	76.8 (25 %)	1,170	−3.9

Purlung	95.71°E, 29.84°N	3,864 (6,052; 2,678)	253.2	17.1 (7%)	2,056	− 2.2

2.3. Evaluation of the automated approach

~~The automatically detected~~ High-resolution multispectral images from RapidEye and PlanetScope were used to manually produce snowline datasets against which to evaluate the automatically detected snowlines. RapidEye and PlanetScope are both Earth observation constellations operated by Planet Labs, with spatial resolutions of 6.5 m and 3.7 m. ~~are~~ We prepared one to three ortho-images for each target catchment that were obtained close to the date when automatic detections were conducted from the Landsat 5/7/8 or Sentinel-2 images. A list of the images used is shown in Table 2.

The automatically detected snowlines were compared with the manually delineated snowlines obtained using high-resolution PlanetScope ortho-images obtained near the date of ~~the~~ automatic ~~detections~~detection (within 10 days). In ~~the~~ manual delineations, the location of the snowline ~~is~~was determined by checking high-resolution satellite images~~,~~ as well as the glacier outline and elevation data ~~and elevation data. Since~~. Because it ~~is~~was difficult to distinguish snowlines on ridges, we ~~create~~created two sets of manually delineated snowlines: (i) snowlines extracted by excluding ridges or shadows (minimum extraction, orange lines in Fig. S3~~)~~), and (ii) snowlines extracted without excluding ridges (maximum extraction~~,~~; blue lines in Fig. S3). We then compare ~~the median values and the cumulative distribution of snowline altitude between the automatically detected and manually delineated snowlines.~~each manually detected snowline point to the nearest automatically detected point in the temporally corresponding Landsat or Sentinel-2 scene, and computed the horizontal and implied vertical distance (based on the DEM) between these two points. We did this for each of 12 validation scenes and for both manual slowline delineations, producing nearly 90’000 evaluation pairs. From these, we determine the median absolute deviations of pairwise distances and height differences for each manual snowline dataset and each scene.

Formatted: Indent: First line: 0.13"

~~To~~In addition, to investigate the agreement of SLAs derived from ~~the~~ different satellites, we ~~compare~~compared the SLAs derived from Landsat 7, Landsat 8, and Sentinel-2 ~~for the period~~ from 2016 to 2019. Landsat 5 ~~is~~data were excluded from this comparison ~~due to its~~because of the operational period (March 1984 to January 2013~~).~~), but we note that the predecessor approach performed favorably for Landsat 5 and 7 scenes (Girona-Mata et al., 2019). This second check is important ~~to determine~~ for determining whether snowlines derived ~~with~~using our method from sensors ~~having~~with different spatial and radiometric resolutions are biased relative to one another (~~e.g.,~~ Rittger et al, 2021).

~~3.3~~2.4. Analysis of ~~results~~

~~We first analyze the~~ SLA seasonality ~~of~~, trends, and controls

We first analysed the seasonality of the SLAs by considering a dual-phase harmonic regression (Eastman, et al, 2009) ~~to~~of the derived SLA values for the full period. The seasonal patterns of SLA in the first (1999~~-~~–2009) and the second (2010~~-~~–2019) half decades are compared using ~~T~~t-tests (significant level ~~α~~= 0.05). For ~~the~~ months with significant differences between the two periods, we ~~examine~~examined the ERA5 climatic factors that could drive the SLA changes.

Formatted: Indent: First line: 0.14"

To examine long-term trends, ~~the~~ satellite-derived SLA values for each scene ~~are~~were converted to a monthly mean. ~~With~~By linearly interpolating the missing values, the 21-year SLA trend ~~is~~was identified using the Mann-Kendall test (significance level ~~α~~ = 0.01). We then examined the climatic factors driving ~~the~~ SLA changes ~~by~~using multiple regression analysis for both annual ~~variation~~variations (12-month moving averages) and longer-term changes (60-month moving averages).

The detected SLA ~~is analyzed~~was analysed to explore the effects of orographic and meteorological controls on seasonal and long-term variations. We ~~investigate~~investigated the disparities in SLA among aspect classes (east-, south-, west-, and north-facing slopes), interpreting the observed differences conceptually using the framework proposed by Girona-Mata et al. ~~(2019). Additionally, we compare the 12-month and 60-month moving averages of SLAs with those of climatic variables (air temperature, precipitation, and solar radiation), assessing their statistical relationships through multiple regression analysis.~~(2019).

~~4~~To further understand the seasonal and long term controls of SLA variations, we analysed climate reanalysis data. We obtained a 0.25° gridded near-surface 2 m air temperature, downward surface shortwave radiation, cloud cover, and precipitation from ERA5 (Hersbach et al., 2020). We aggregate the hourly products into daily and monthly mean datasets. The air temperature was corrected to the average snowline altitude during the target period (1999 –2019) in each catchment using a standard environmental lapse rate (0.065 °C m-1). Finally, we compared the 12-month and 60-month seasonal decomposition of the SLAs with those of climatic variables (air temperature, precipitation, and solar radiation) and assessed their statistical relationships through multiple regression analysis. For this trend analysis, we use a Seasonal Trend Decomposition based on Loess (STL) method, which is typically a robust trend detection method for noisy data with variable sampling and strong seasonality (Cleveland et al, 1990).

3 Results

3.1. ~~4.1. Snowline evaluation~~

Evaluation of detected snowlines

We first ~~compared~~present the comparison of detected SLAs from our method with those obtained through manual delineation at multiple scenes in each catchment~~, evaluating~~ to indicate the ~~reasonableness~~accuracy of the detected SLA. The SLAs obtained from our method ~~exhibit strong~~exhibited a very close agreement with the manual delineation results ~~for most of the scenes~~ (Table 2~~); excellent agreement in 3 scenes (),~~ with ~~a difference in SLA < 20m), good agreement in 6 scenes (20m < difference < 200m), and fair agreement in 2 scenes (200m < difference). The SLAs of~~median absolute horizontal distances below 25 m for nearest snowline points in all scenes, and median absolute vertical distances (SLA differences) of 10m or less. The spatial correspondence of the derived snowlines from automatic and manual methods was superb (Fig. S8-9 for examples) for areas of overlapping coverage. Interestingly, despite this close correspondence, the cumulative distributions of snowline elevations differed substantially between the automatic and manual snowline derivations (Fig S10) highlighting the importance of consistent catchment-wide sampling of snowline elevations. This is achievable through automated processing but not through manual delineation ~~used in the above comparison refer to the average of two manual delineation results (maximum and minimum delineations, see Section 3.2). Subsequently,~~; we ~~compared the cumulative frequency of altitude at each grid on the snowlines between the automatically and manually detected snowlines (Fig. S3). As depicted in Figure S3, the three scenes demonstrating excellent agreement also exhibit remarkably consistent cumulative distributions, whereas the two scenes with fair agreement reveal a bias in the automatic detection results toward higher altitudes. The potential cause of the bias toward high altitude will be discussed in Section 5.3. For the remaining scenes (6 scenes with good agreement), some variations in cumulative frequency are observed; however, these differences are relatively minor and do not significantly affect the final SLA value, which represents the median of all detected altitudes on~~note that in situ monitoring of snowlines ~~in one scene. The scenes with fair agreement highlight that the method successfully identifies snow cover boundaries at high elevation that are often ignored by manual operators; in most cases this~~

~~results in a slightly higher statistical snowline altitude than the manual operators identify~~(e.g. Moringa, Seko, and Takahashi, 1987) can thus provide rich information about temporal variability of snowlines, but may be locally biased in terms of the SLA.

Considering the ~~inter-satellite~~intersatellite variability between the SLAs retrieved from Landsat 7, Landsat 8, and Sentinel-2 (Fig. S4), we observed the least variation in SLAs during the monsoon season (with a standard deviation σ of SLA for all sites and satellites < 18 m) and the largest variation during winter (σ < 140 m). ~~The disagreements~~Disagreements during winter ~~are~~were not unexpected~~,~~ given the inconsistent acquisition dates for the three satellites and the variable occurrence of winter snowfall in the Himalayas. Focusing on the differences in snowline altitudes (SLAs) ~~among~~between different satellites during the monsoon season, we ~~observe~~observed a high degree of consistency in the range of SLA values within each catchment. Despite ~~the~~ heavy cloud cover, the standard deviation in the median SLA between different satellites generally ~~remains~~remained within 50 m, except for Parlung, where the deviation ~~extends~~extended to 120 m. ~~While~~Although these variations may appear significant, they are relatively minor compared to the seasonal SLA variations observed for each sensor. Therefore, we consider the bias resulting from the use of different satellites in this study to be acceptable for examining seasonal and decadal changes in the SLA.

~~**Table 2: Comparison of snowline altitudes (m a.s.l.) between the automatic detection and manual delineation. The SLA from manual delineation is the average value of two types of manual delineation results, with the maximum and minimum delineation results shown in square brackets after the average value. The data acquisition dates and used satellites are shown in brackets.**~~

Table 2: Performance of the automated snowline in comparison to manually digitized snowline datasets 1 and 2, reporting the median absolute deviation (MAD) for horizontal distances (D) and vertical differences (H) of nearest pairs of snowline points in the dataset.

Catchment	~~SLA from~~Scene for automatic detection	~~SLA from~~Scene for manual delineation	~~Difference~~MAD D1 (m)	MAD H1 (m)	MAD D2 (m)	MAD H2 (m)
Satopanth	~~5,330~~ ~~(~~September 13, 2017, Landsat 8~~)~~	~~5,479 [5,445; 5,513]~~ ~~(~~September 13, 2017, RapidEye~~)~~	~~149~~16	9	16	7
	~~4,634~~ ~~(~~January 20, 2021, Landsat 8~~)~~	~~4,440 [4,726; 4,154]~~ ~~(~~January 27, 2021, PlanetScope~~)~~	~~194~~16	9	16	7
Hidden Valley	~~5,530~~ ~~(~~June 15, 2019, Sentinel-2~~)~~	~~5,536 [5,509; 5,564]~~ ~~(~~June 15, 2019, PlanetScope~~)~~	~~6~~10	3	9	3
	~~5,387~~ ~~(~~May 25, 2020, Sentinel-2~~)~~	~~5,406 [5,371; 5,441]~~ ~~(~~May 23, 2020, PlanetScope~~)~~	~~19~~10	3	10	3
	~~5,675~~ ~~(~~October 12, 2020, Sentinel-2~~)~~	~~5,498 [5,455; 5,540]~~ ~~(~~October 12, 2020, PlanetScope~~)~~	~~177~~10	3	9	2
	December 30, 2020, Sentinel-2	December 30, 2020, Sentinel-2	11	3	10	3
Langtang	~~4,615~~ ~~(~~February 12, 2016, Landsat 8~~)~~	~~4,497 [4,457; 4,538]~~ ~~(~~February 13, 2016, RapidEye~~)~~	~~118~~15	7	15	6
	~~4,665~~ ~~(~~November 13, 2017, Landsat 8~~)~~	~~4,555 [4,443; 4,668]~~ ~~(~~November 12, 2017, RapidEye~~)~~	~~110~~15	6	17	8
Rolwaling	~~5,213~~ ~~(~~December 30, 2019, Landsat 8~~)~~	~~4,946 [5,067; 4,825]~~ ~~(~~December 30, 2019, PlanetScope~~)~~	~~267~~22	10	19	8
	~~4,621 (April 20, 2020, Landsat 8)~~	~~4,285 [4,367; 4,202] (April 19, 2020, PlanetScope)~~			~~336~~	
	~~4,892~~	~~4,881 [4,802; 4,961]~~	~~11~~18	8	17	8

Inserted Cells
Formatted: Font: Times New Roman
Formatted: Font: Times New Roman
Inserted Cells
Inserted Cells
Formatted: Font: Times New Roman
Formatted: Font: Times New Roman
Formatted ...
Formatted ...
Formatted: Font: Times New Roman
Formatted: Font: Times New Roman
Formatted ...
Formatted ...
Formatted: Font: Times New Roman
Formatted ...
Formatted ...
Formatted: Font: Times New Roman
Formatted: Font: Times New Roman
Formatted ...
Formatted ...
Formatted: Font: Times New Roman
Formatted ...
Formatted ...
Formatted: Font: Times New Roman
Inserted Cells
Inserted Cells
Inserted Cells
Formatted ...
Formatted ...
Formatted: Font: Times New Roman
Formatted: Font: Times New Roman
Formatted ...
Formatted ...
Formatted: Font: Times New Roman
Formatted: Font: Times New Roman
Formatted ...
Formatted ...
Formatted: Font: Times New Roman
Split Cells
Inserted Cells
Inserted Cells
Formatted: Font: Times New Roman
Formatted: Font: Times New Roman
Inserted Cells

	~~(~~May 17, 2020, Sentinel-2~~)~~	~~(~~May 27, 2020, PlanetScope~~)~~				
Parlung	~~3,841~~ ~~(~~December 29, 2020, Landsat 8~~)~~	~~4,012 [4,012; 4,013]~~ ~~(~~December 29, 2020, PlanetScope~~)~~	~~17~~20	10	20	9
Mean			15	6	14	6

~~4~~3.2. ~~Seasonality~~Snowline seasonality

~~Figure 2 shows the~~ The derived SLA values ~~over the year, demonstrating~~demonstrate strong seasonal variability ~~despite considerable intraseasonal spreads. Despite the relatively smaller number of acquired images during the monsoon period at all sites due to thick cloud cover, the derived SLAs for this period exhibit close agreement.~~(Figure 3). Across most sites, ~~two peaks in~~ SLA ~~are~~maxima were observed during the monsoon and minima in the winter ~~seasons~~season, which ~~are~~is consistent with the findings of Girona-Mata et al. (2019). ~~The double-peak is more evident in Satopanth, Rolwaling, and Hidden Valley, located at high-elevation but monsoon-dominated sites. A prominent peak during the monsoon is observed in Langtang Valley, while one moderate peak is noted in Parlung.~~

~~At all sites, the SLA reaches its maximum during the monsoon season, but~~However, the timing of the ~~peak varies~~maximum SLA varied slightly among the sites: July in Langtang~~,~~ and August in Satopanth, Rolwaling, and Parlung. Hidden Valley ~~shows~~showed a relatively stable SLA during the monsoon season, with a less pronounced maximum ~~peak~~SLA occurring in August (Fig. ~~2f~~3f). The minimum SLA ~~occurs~~occurred in late winter or early pre-monsoon ~~for~~at all sites: January in Langtang, February in Hidden Valley, March in Rolwaling and Parlung, and April in Satopanth. The winter-spring SLA ~~in~~transition differed between sites: at Langtang ~~begins~~SLA began to increase in January, ~~while~~whereas the SLA ~~in~~at Satopanth ~~continues~~continued to decrease until April. ~~Parlung shows~~All sites exhibited a relatively ~~flat~~steady winter SLA. The differences between the minimum ~~and maximum SLAs ~~vary~~varied from 480 m (Hidden Valley) to 1,100 m (Langtang).~~

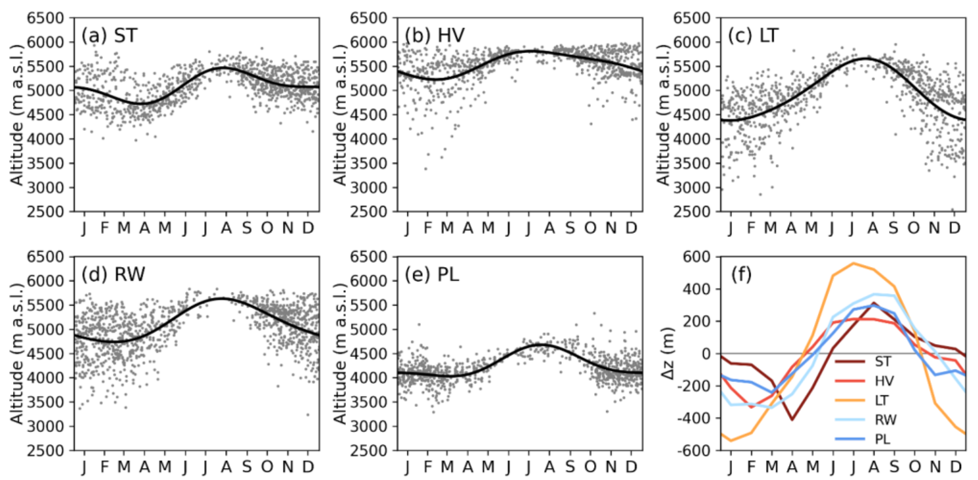

Formatted: Font: Times New Roman
Formatted: Font: Times New Roman
Formatted: Font: Times New Roman
Formatted: Font: Times New Roman
Formatted: Font: Times New Roman
Formatted: Font: Times New Roman
Formatted: Font: Times New Roman
Formatted: Font: Times New Roman
Formatted: Font: Times New Roman
Formatted: Font: Times New Roman
Formatted: Indent: First line: 0.13"

All sites show strong intraseasonal dispersion in wintertime, when the range of SLA measurements is greater than the annual SLA amplitude; the winter SLA range doubles the annual amplitude at Hidden Valley, Langtang, and Rolwaling. Despite the relatively small number of images acquired during the monsoon period at all sites due to thick cloud cover, the derived SLAs for this period exhibit narrow spread and the highest SLA values. In all catchments other than Parlung, the monsoon-period SLA exceeded 5500 m a.s.l.; in Parlung, the ice-free topographic availability limited snowline retrievals to 5000 m a.s.l. As noted by Girona-Mata et al., (2019), we find a strong second harmonic phase in Satopanth, Rolwaling, and Hidden Valley, which are located at high elevation but monsoon-dominated sites. This second harmonic was less prominent in Langtang Valley and in Parlung.

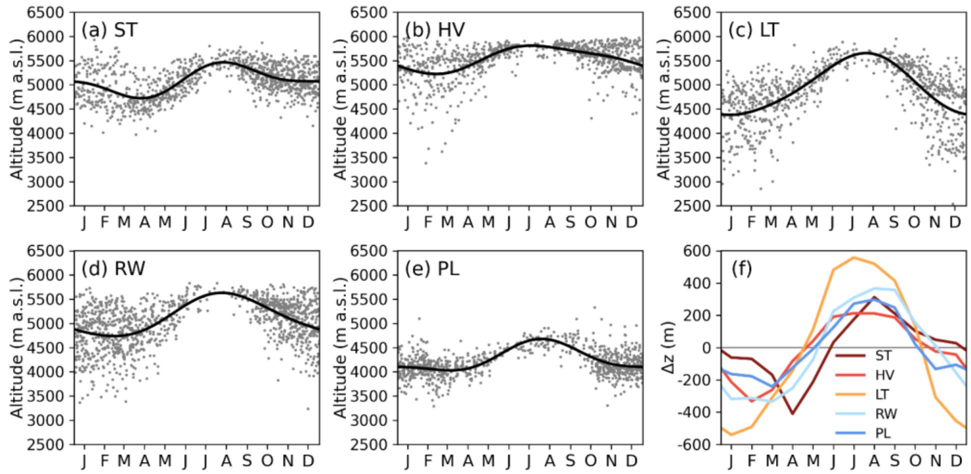

Figure ~~2~~3: (a)-(e) The derived ~~snow line~~snowline altitude (SLA) over the target period (1999-2019) at each catchment and (f) the SLA anomaly from the mean SLA over the target period (1999-2019). Grey dots and solid lines in (a)-(e) show the SLAs derived from each satellite scene and smooth curves fitted with harmonic functions, respectively. Catchment abbreviations denote ST: Satopanth, HV: Hidden Valley, LT: Langtang, RW: Rolwaling, and PL: Parlung, respectively.

~~4.~~

3. ~~Trend~~3. Trends in ~~mean~~ SLA 1999-2019

The STL time series decomposition of SLAs ~~shows regionally different~~revealed contrasting SLA trends between catchments (Fig. ~~3~~4). Increasing SLA trends ~~of SLA are~~were found in Hidden Valley (+11.9 m yr^{-1}), Langtang ~~Valley~~ (+14.4 m yr^{-1}), and Rolwaling ~~Valley~~ (+8.2 m yr^{-1}~~)~~), whereas Satopanth ~~shows~~showed a decreasing trend (−15.6 m yr^{-1}) and Parlung ~~shows~~showed no statistically significant trend (Fig. ~~3~~4). These trends were confirmed for both 12-month and 60-month moving averages using the Mann-Kendall test, and the p-values for the four catchments where trends were detected were all less than 0.001. The ~~elevation~~altitudinal difference between the minimum and maximum SLAs, with 12-month moving averages for each catchment ~~varies from~~, varied between 580 m (Parlung) ~~to~~and 820 m (Langtang).

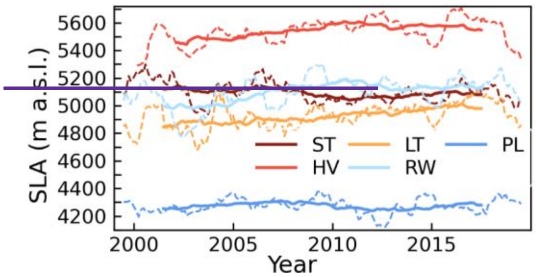

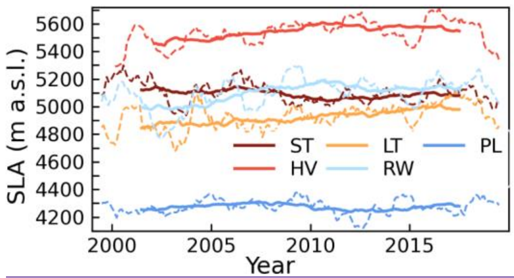

Figure ~~3: Snow line~~4: Snowline altitude with 60-month (solid lines) and 12-month (dashed lines) moving averages at the five target catchments. ~~Trends are listed in Table 1.~~ Catchment abbreviations denote ST: Satopanth, HV: Hidden Valley, LT: Langtang, RW: Rolwaling, and PL: Parlung, respectively. Trends ($p<0.001$) for the moving averages were ST: -15.6 m yr^{-1}; HV: 11.9 m yr^{-1}; LT: 14.4 m yr^{-1}; RW: 8.2 m yr^{-1}; PL: insignificant.

Formatted: Font: 10 pt, Not Bold, Font color: Auto

Formatted: Space After: 10 pt, Border: Top: (No border), Bottom: (No border), Left: (No border), Right: (No border), Between : (No border)

~~4~~3.4. Seasonal SLA aspect differences

~~The~~Catchment snowlines showed ~~distinctive~~distinct seasonal patterns of ~~SLA~~ aspect dependence (Fig. ~~4~~5). A common characteristic among the five catchments ~~is~~was the minimal difference in SLA between aspects during the monsoon season, ~~contrasting with~~in contrast to the substantial SLA differences between aspects during ~~the~~ winter. Additionally, the standard deviation in the SLA, represented by the error bars in Fig. ~~4, is~~5, was smallest during the monsoon season, gradually increasing, and largest during winter. Regarding specific regional characteristics, Satopanth ~~shows~~showed minimal differences in the SLA between aspects, even during winter, with only a slight decrease in the north-facing SLA. Conversely, ~~in the Parlung region,~~ aspect-induced differences ~~are~~were pronounced throughout the year~~.~~ in the Parlung region. Furthermore, Parlung ~~exhibits~~exhibited a relatively small seasonal variability in the standard deviation of the SLA values.

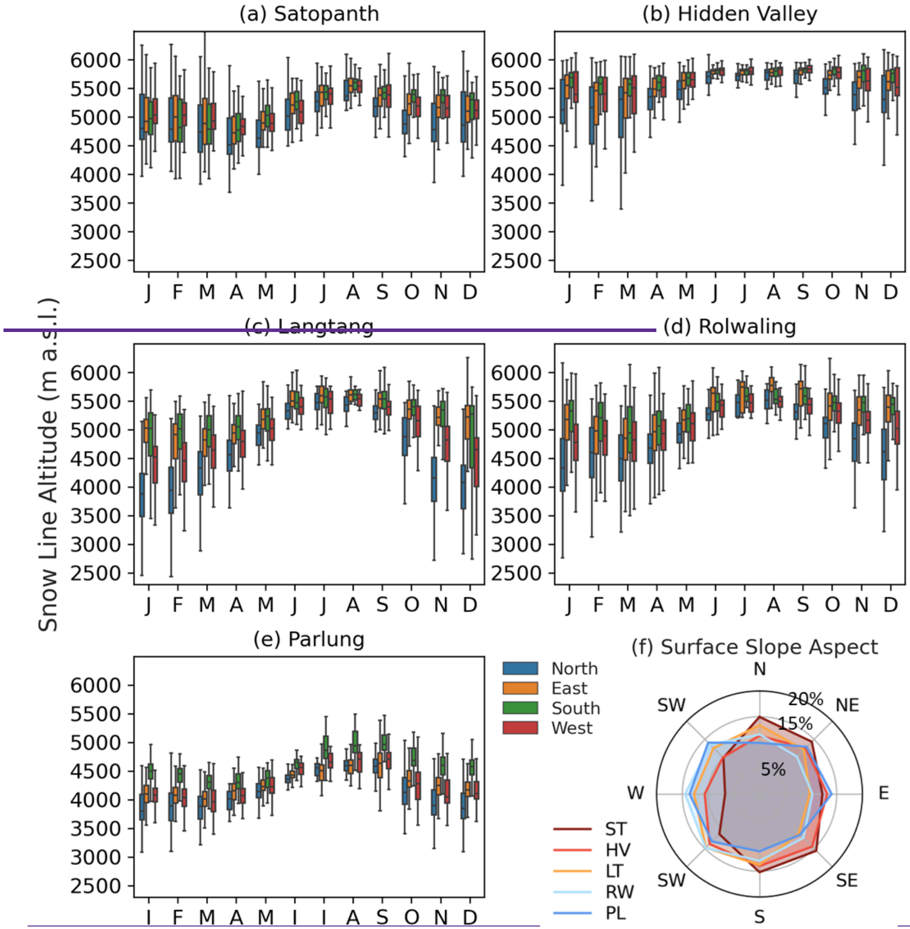
(a) Satopanth
(b) Hidden Valley
(c) Langtang
(d) Rolwaling
(e) Parlung
(f) Surface Slope Aspect
Snow Line Altitude (m a.s.l.)
6000
5500
5000
4500
4000
3500
3000
2500
J F M A M J J A S O N D
North
East
South
West
N
NE
E
SE
S
SW
W
SW
20%
15%
5%
ST
HV
LT
RW
PL

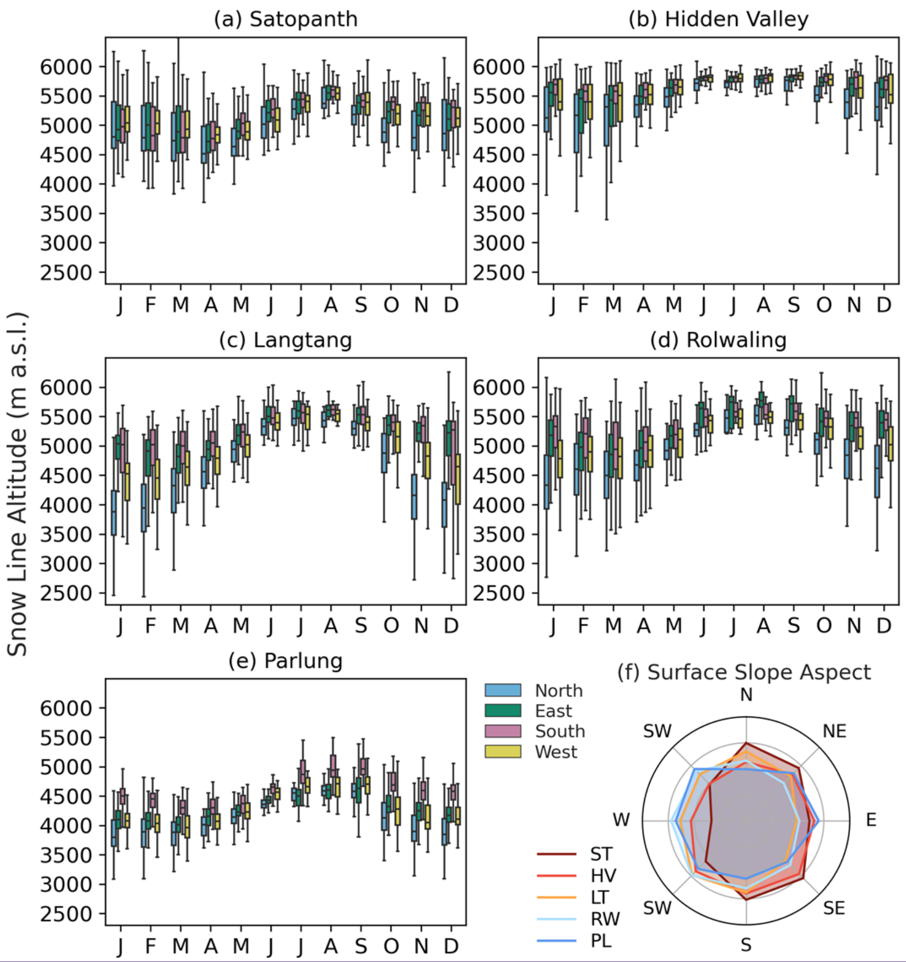

Figure ~~4~~5: (a)-(e) Boxplots of monthly ~~snow line~~snowline altitude (SLA) for each aspect of the slope; north, east, south, and west. (f) Relative distribution of 45-degree topographic aspects for each catchment (%).

~~4~~3.5. Decadal changes in seasonal SLA

To examine the cause of the long-term changes in the SLA shown in Fig. ~~3~~4, we compared the seasonal patterns of the SLA and climatic variables for the first half (1999-2009 in blue) and ~~the~~ second half (2010-2019~~) periods at~~ in red) of each catchment (Fig. ~~5~~6). Focusing on the months with statistically significant ~~change~~changes, SLA decreases ~~are~~were found in March in Satopanth (Fig. ~~5a~~6a), Hidden Valley (Fig. ~~5b~~6b), and Rolwaling (Fig. ~~5d),~~6d) and in January in Parlung (Fig. ~~5e~~6e). No significant seasonal SLA decrease ~~is found in~~ was observed at Langtang (Fig. ~~5c~~6c). Increases in the SLA ~~are~~were evident in September in Satopanth (Fig. ~~5a~~6a), October to December in Hidden Valley (Fig. ~~5b~~6b), July and October in Langtang (Fig. ~~5c~~6c), and July, October, and

November in Rolwaling (Fig. ~~5d~~6d). No significant increase ~~is found~~was observed in Parlung (Fig. ~~5e~~6e). Overall, ~~the~~ SLA decreases ~~are~~were primarily detected in winter to early spring, and ~~the~~ increases in the monsoon and post-monsoon seasons.

The ~~lowering~~decrease of winter SLA ~~can be attributed to the~~is associated with a decrease in ~~temperatures~~temperature in January across all regions where ~~the~~a decrease ~~of~~in winter SLA ~~is~~was detected. The increase in precipitation during February and March may also ~~contributes~~have contributed to the lowering of winter SLAs in Satopanth, Hidden Valley, and Rolwaling. No changes in solar radiation ~~are observed that could be related~~were identifiable in relation to decreases in the ~~decrease in~~ winter SLA. ~~On the other hand, the~~

The rising SLAs identified in the three Nepalese catchments (Hidden Valley, Langtang, and Rolwaling) ~~are likely due to~~ were all associated with rising temperatures during the monsoon~~, which has had a stronger effect on seasonal~~. We note that the SLA ~~than both~~increases occurred in conjunction with precipitation ~~increase~~ increases (all three sites) and net shortwave ~~decrease. Although the increase in precipitation~~decreases (all except Rolwaling). Consequently, the SLA variations during the monsoon ~~season is also statistically significant in these three catchments, the SLA during the monsoon is controlled by the snow/rain transition altitude which is determined by the altitude dependence of~~ may be more closely linked to air temperature ~~(discussed in Section 5.1). It thus seems plausible that the increase in temperature is the main factor contributing to the SLA increase during the monsoon and the post-monsoon.~~than to precipitation, shortwave radiation, or cloud cover. The decrease in solar radiation during the monsoon ~~is~~was statistically significant in the three Nepalese ~~three~~ regions which ~~could be~~is consistent with ~~the~~ increased precipitation. It is unrealistic ~~that~~for the decrease in solar radiation ~~contributes~~to contribute to the ~~SLA~~ increase in SLA, but it could suppress the increasing rate of the SLA. ~~On the contrary~~In contrast, the increasing solar radiation in November in Rolwaling may ~~contribute~~have contributed to the ~~SLA~~ increase in the SLA in the same month. In Satopanth, ~~the SLA~~an increase is ~~only~~ observed only in September, suggesting an association with the temperature increase in the same month.

Formatted: Font color: Auto
Formatted: Font color: Auto
Formatted: Font color: Auto
Formatted: Font color: Auto
Formatted: Font color: Auto
Formatted: Font color: Auto
Formatted: Font color: Auto
Formatted: Font color: Auto
Formatted: Font color: Auto
Formatted: Font color: Auto
Formatted: Font color: Auto
Formatted: Font color: Auto
Formatted: Font color: Auto
Formatted: Font color: Auto
Formatted: Font color: Auto
Formatted: Font color: Auto
Formatted: Font color: Auto
Formatted: Font color: Auto
Formatted: Font color: Auto
Formatted: Font color: Auto
Formatted: Font color: Auto
Formatted: Font color: Auto
Formatted: Font color: Auto
Formatted: Font color: Auto
Formatted: Font color: Auto
Formatted: Font color: Auto
Formatted: Font color: Auto
Formatted: Font color: Auto
Formatted: Font color: Auto
Formatted: Font color: Auto
Formatted: Font color: Auto
Formatted: Font color: Auto
Formatted: Font color: Auto
Formatted: Font color: Auto
Formatted: Font color: Auto
Formatted: Font color: Auto
Formatted: Font color: Auto
Formatted: Font color: Auto
Formatted: Font color: Auto

404 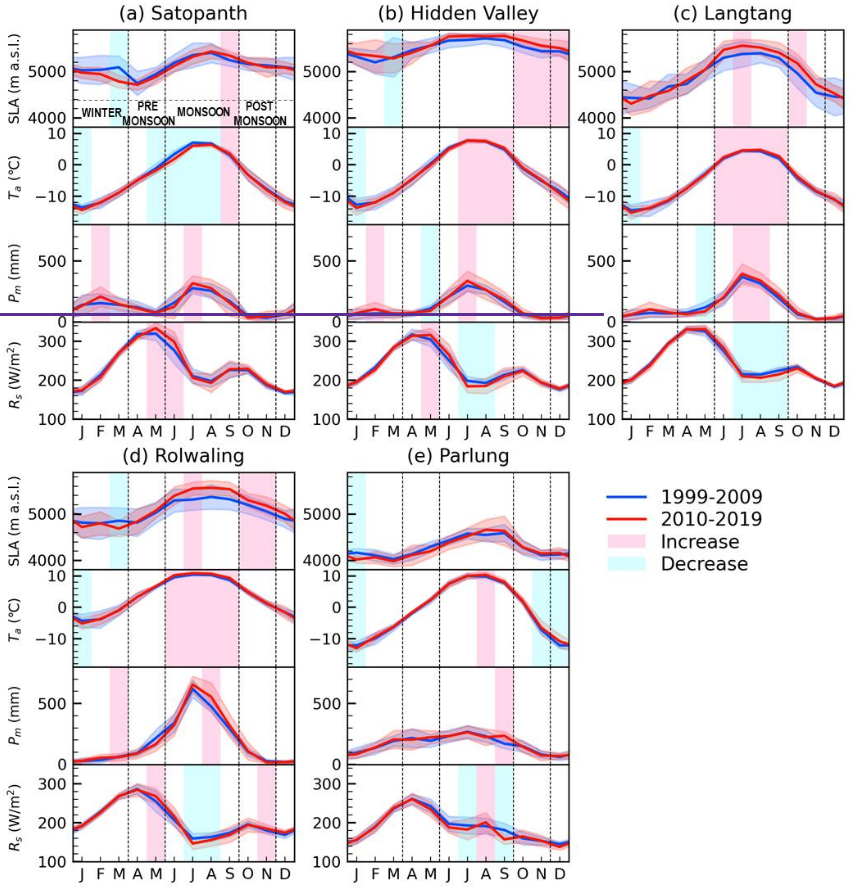

(a) Satopanth
(b) Hidden Valley
(c) Langtang
(d) Rolwaling
(e) Parlung
SLA (m a.s.l.)
T_a (°C)
P_m (mm)
R_s (W/m^2)
WINTER
PRE MONSOON
MONSOON
POST MONSOON
J F M A M J J A S O N D
1999-2009
2010-2019
Increase
Decrease

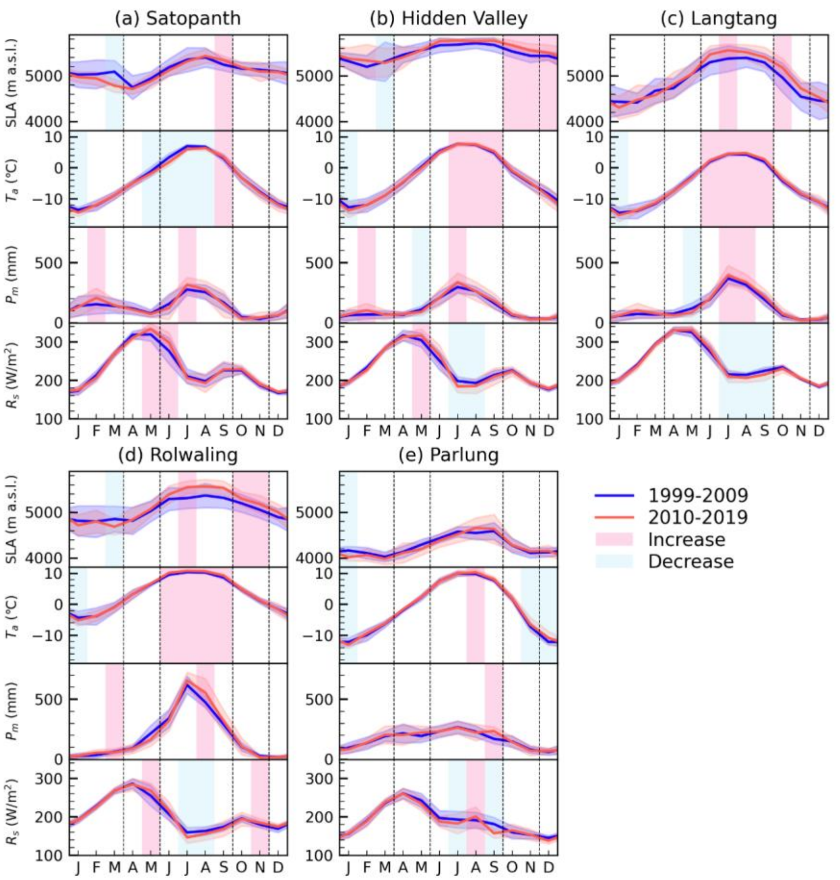

Figure ~~5~~6: Monthly climatologies of SLA and climate variables (Ta: air temperature at 2-m height, Pm: monthly total precipitation, and Rs: daily mean downward solar radiation flux at the surface) for the first half (1999-2009 in blue) and the second half (2010-2019 in red), respectively. Shaded areas indicate statistically significant changes (pink for the increase and light blue for the decrease) between the periods.

~~4~~3.6. ~~Controlling factors for decadal~~ Relationships between trends in meteorology and SLA

The 12-month moving averages of snowline altitude ~~(SLA) exhibit~~exhibited significant correlations with changes in air temperature across most sites, except for Satopanth (Fig 7, Table 3). In Rolwaling, all ~~three~~ climatic variables ~~demonstrate an influence on~~except precipitation demonstrated a correlation with the SLA, with air temperature exhibiting the strongest impact, as evidenced by the largest t-value. Conversely, in Satopanth, precipitation ~~emerges~~emerged as the sole ~~influencing factor~~statistical control on SLA, with a negative t-value~~,~~ indicating that ~~the~~ precipitation ~~works to lower~~lowers the SLA. This finding that increased precipitation ~~lowers~~at the decadal scale has lowered the SLA is consistent with the results of ~~Section 4.5~~our seasonal analyses that ~~increasing~~increased winter snowfall ~~has acted to lower~~ lowers the winter SLA at Satopanth.

Overall, our results underscore the substantial influence of air temperature on SLA variations, which is consistent with previous research (Girona-Mata et al, 2019; Tang et al., 2020). This relationship is also expected to ~~be the decisive~~decisively control ~~of~~ future snow climatology in the region (Kraaijenbrink et al., 2021). However, we also ~~find~~found that winter precipitation can serve as a significant driving factor, particularly ~~evident~~ in Satopanth, where the SLA displays a ~~decreasing~~negative trend~~. While~~ over our study period. Although the influence of solar ~~radiation's influence is relatively~~radiation is smaller ~~compared to~~than that of air temperature, it contributes to an increase in the SLA in Rolwaling. We also note that cloud cover plays a significant role and is negatively correlated to SLA for both Hidden Valley and Langtang.

Formatted: Indent: First line: 0.13"

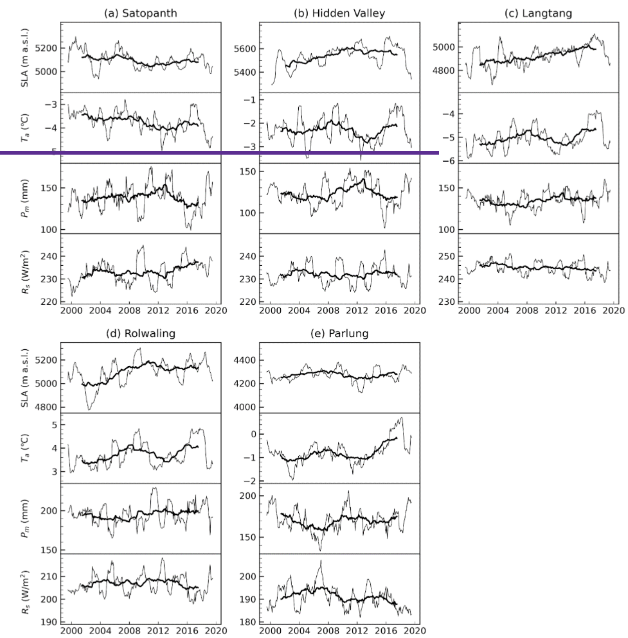

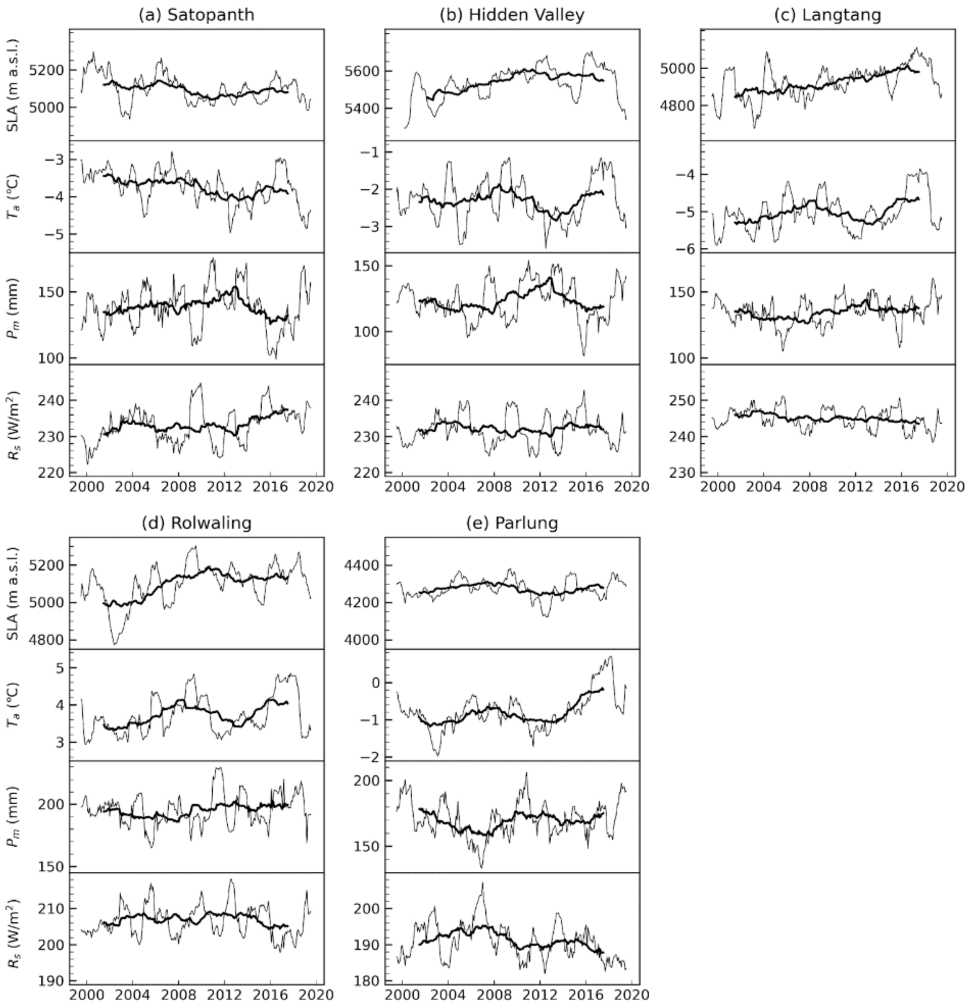

Figure ~~5~~7: Time series of SLA and climate variables (Ta: air temperature at 2-m height, Pm: monthly total precipitation, and Rs: daily mean downward solar radiation flux at the surface) for the period from 1999 to 2019. Variables with 60-month and 12-month moving averages are drawn with thick and thin lines, respectively.

~~**Table 3: Results**~~

Table 3: Correlation coefficients (R) between SLAs and single variables calculated using 12-month and 60-month moving averages, and results of the multiple regression analysis using 12-month moving averages of climate data and SLA. Influential factors (p-value < 0.05 and |t-value| > 2.0) are shown in bold. A positive or negative t-value indicates a contribution to the increase or decrease of SLA, respectively.

		Univariate		Multivariate			
		12-month R (p-value)	60-month R (p-value)	Coefficient	Standard error	t-value	p-value
Satopanth	Air temperature	0.50 (<0.001)	0.80 (<0.001)	6.~~14~~05	11.~~07~~18	0.~~56~~54	0.~~579~~580
	Precipitation	~~−2.82~~ − 0.18 (0.004)	− 0.44 (<0.001)~~36~~	− 2.81	0.39	− ~~−~~7.~~89~~24	**<0.001**
	Solar radiation	~~−1.18~~ − 0.44 (<0.001)	− 0.11 (0.129)	− 11.85	**1.17**	~~−1.01~~ − 10.12	<0.~~108~~001
	Cloud cover	− 0.15 (0.017)	− 0.34 (<0.001)	− 0.13	1.97	− 0.07	0.948
Hidden Valley	Air temperature	~~52.42~~0.34 (<0.001)	− 0.07 (0.34)	68.26	**12.**~~06~~82	~~4.35~~5.32	**<0.001**
	Precipitation	− ~~−~~0.~~40~~21 (<0.001)	0.~~61~~51 (<0.001)	~~−~~0.~~65~~10	0.~~516~~62	0.17	0.869
	Solar radiation	~~1.54~~0.04 (0.51)	− 0.36 (<0.001)	5.56	**2.**~~14~~45	~~0.72~~2.27	**0.**~~472~~024
	Cloud cover	0.05 (0.47)	0.18 (0.017)	10.52	3.29	3.20	0.002
Langtang	Air temperature	~~95.14~~0.57 (<0.001)	~~11.28~~0.45 (<0.001)	~~8.44~~94.58	12.49	7.58	**<0.001**
	Precipitation	− ~~−~~0.~~33~~08 (0.207)	0.~~77~~59 (<0.001)	− 0.34	0.78	− ~~−~~0.43	0.~~669~~667
	Solar radiation	~~−2.84~~ − 0.19 (0.003)	− 0.69 (<0.001)	− 2.~~98~~81	~~−1.01~~3.12	− 0.95~~314~~	0.341
	Cloud cover	− 0.13 (0.037)	− 0.15 (0.031)	− 0.39	3.68	− 0.11	0.916

Rolwaling	Air temperature	~~147.57~~0.61 (<0.001)	~~11.33~~0.71 (<0.001)	87.45	13.~~03~~19	6.63	<0.001
	Precipitation	~~2.83~~0.01 (0.864) ~~0.71~~ ~~4.00~~	~~<0.40~~ (<0.001)	0.74	0.70	1.06	0.290
	Solar radiation	~~9.95~~ − 0.05 (0.410)	0.11 (0.146)	− 8.47	3.23	− 2.63 20	~~4.52~~0.009 ~~<0.001~~
	Cloud cover	− 0.40 (<0.001)	− 0.76 (<0.001)	− 32.63	4.50	− 7.26	<0.001
Parlung	Air temperature	~~30.37~~0.28 (<0.001)	0.43 (<0.001)	~~83~~2.41	~~3.65~~7.71	~~<0.001~~4.20	<0.001
	Precipitation	− ~~−~~0.~~29~~15 (0.019)	− 0.67 (<0.001)~~24~~	− 0.43	0.40	− ~~−~~1.~~21~~08	0.~~227~~286
	Solar radiation	0.~~99~~04 (0.549)	0.~~78~~58 (<0.001)	1.~~28~~34	~~0.201~~1.34	1.00	0.317
	Cloud cover	− 0.06 (0.334)	− 0.51 (<0.001)	3.09	2.66	1.16	0.248

~~5~~4 Discussion

~~5~~4.1. Seasonal pattern & controls

We found ~~both consistency~~consistencies and differences in the seasonal patterns across the five target catchments. Across the five regions, the SLA reaches its highest level during the monsoon summer~~,~~ and is maintained at ~~the~~a relatively stable snow/rain transition altitude caused by ~~the~~ abundant precipitation and ~~the~~ altitude dependence on air temperature (Girona-Mata et al., 2019). Once the precipitation reaches a sufficient level to maintain this altitude, additional precipitation has no further impact on the SLA. Solar radiation is less effective during the monsoon summer ~~due to the~~because of frequent and heavy cloud cover~~ which leads~~, leading to highly diffused shortwave radiation (Pellicciotti et al., 2011). However, Parlung ~~is~~was an exception, as indicated by the minimal differences in SLA between the aspects (Fig. ~~4~~5). In Parlung, differences in SLA between aspects ~~persist~~persisted even in summer (Fig. ~~4~~5), suggesting that solar radiation still has an impact on SLA.

Snow is most abundant from late winter to early pre-monsoon, just before the snowmelt begins in earnest. In Langtang, SLA shows the ~~lowest peaks~~seasonal minimum in January, indicating snowmelt starting in February as solar radiation increases. In contrast, Satopanth experiences a later ~~peak~~minimum, seeing the lowest SLA in April. This region is less influenced by solar radiation throughout the year (Fig. ~~4~~5), so snowmelt may begin primarily when temperatures rise.

Winter exhibits significant variability in the snowline altitude (SLA) across ~~the~~ catchments~~, largely due to the influence of westerly storms. These~~. Winter storms sporadically ~~bring heavy snowfall~~deposit snow to very low elevations, which then ablates to the seasonal freezing line, leading to increased variability in the SLA. The cumulative likelihood of these storms increases throughout the winter, such that the seasonal snowline eventually converges to approximate the freezing line before the monsoon. Particularly ~~in~~at Langtang and Rolwaling, the variability ~~is~~was pronounced, with more snow cover on the west-facing slopes ~~compared to~~than on the east-facing slopes~~, indicating the impact of westerly winds~~ (Fig. ~~4~~5). Conversely, Hidden Valley experiences less east-west variation and ~~less~~ winter SLA variability ~~compared to~~than Langtang and Rolwaling. This could be attributed to ~~the presence of~~ the high-altitude Dhaulagiri mountain range to the southwest, which may act as a barrier to westerly winds, thereby limiting the inflow of moist air across the mountains. Despite being located further west, Satopanth ~~exhibits~~exhibited minimal ~~east-west~~aspect variation in the SLA~~.~~ (Fig. 5). The Satopanth catchment features high-elevation ridges on its western side (Fig. 1).

Therefore, westerly winds (Cannon et al., 2015; Maussion et al, 2014) may ~~deposit~~have deposited more snow on the outer western slopes of the catchment area. It is conceivable that winds crossing ~~over~~ these western ridges ~~contribute~~contributed to snowfall within the catchment. This phenomenon may explain the reduced east-west disparity observed in Satopanth compared to regions directly impacted by prevailing winds. In contrast, Parlung, located on the southeastern Tibetan Plateau, ~~experiences~~is less ~~influence from~~influenced by westerly winds. Based on the above analysis, the seasonal patterns of ~~the~~ SLA are not only dependent on climatic factors but are also significantly influenced by topography.

~~5~~4.2. Trends, decadal changes in seasonality, and controls

~~The long~~Long-term trends and statistically significant explanatory variables ~~exhibit~~exhibited similar patterns in ~~nearby regions~~the study catchments (Fig. ~~3~~7). Satopanth ~~shows~~showed a declining SLA trend, primarily ~~driven by~~associated with the trend in ERA5 precipitation. In contrast, the three Nepalese ~~regions exhibit~~catchments exhibited increasing SLA trends~~,~~ that were mainly ~~influenced by~~ associated with temperature. Parlung ~~shows~~showed no discernible trend, with fluctuations that were possibly related to temperature variations.

Formatted: Indent: First line: 0"

~~Based on the results presented in section 4.5, we~~We interpreted ~~which monthly~~the seasonal meteorological changes ~~are~~ driving ~~the~~ long-term variations in SLA. In Satopanth, the declining trend ~~is~~was primarily driven by a decrease in SLA in March. This ~~March SLA~~ decrease in SLA in March could be attributed to increased snowfall in February~~,~~ following a temperature decrease in January. This finding is consistent with ~~the~~that of a previous study~~, which~~ that reported ~~a rising~~an increasing trend of synoptic-scale Western Disturbance activity over the past few decades, leading to increased winter precipitation in the western Himalayas (Krishnan et al., 2019). Conversely, the rising SLA in September may ~~moderate~~have moderated the ~~lowering~~decreasing rate of the interannual trend of SLA in Satopanth. In the three Nepalese regions, the increasing trends of SLA are driven by SLA increase during the monsoon to post-monsoon period, corresponding to rising temperatures during the monsoon season. ~~Hidden Valley and Rolwaling also exhibit SLA lowering in March, possibly attributed to increased winter precipitation. As for Parlung, a decrease in SLA due to lower temperatures in January is observed. However, this January SLA decrease is not enough to cause a long-term trend of declining SLA.~~The rising temperatures during the monsoon had a stronger effect on SLA than concurrent precipitation increases and net shortwave decrease. Although the increase in precipitation during the monsoon season is also statistically significant in these three catchments, the SLA during the monsoon may be controlled by the snow/rain transition altitude which is determined by the altitude dependence of air temperature, generalizing past inferences for Langtang by (Girona-Mata et al., 2019) to the Central Himalaya. It thus seems plausible that the increase in temperature is the main factor contributing to the SLA increase during the monsoon and the post-monsoon

Hidden Valley and Rolwaling also exhibited SLA lowering in March, possibly attributed to increased winter precipitation. In Parlung, a decrease in SLA due to lower temperatures was observed in January. However, this decrease in the January SLA was not sufficient to cause a long-term trend of declining SLA.

We anticipate that the long-term SLA trend ~~of SLA~~ is controlled by the balance between ~~the~~ increased snowmelt during the monsoon and increased snowfall during winter. The balance between winter precipitation and summer temperature varied among the five catchments~~,~~ despite being located in the same Himalayan range. ~~Those~~These results indicate that regions with different climatic and topographic characteristics, such as arid areas or those with winter accumulation, ~~could~~may have distinct factors controlling snow cover variability.

~~5.3. Limitations, advantages, and future perspectives~~

~~In our analysis, the largest discrepancy (7%) between the automated and manual extraction of snowline altitude (SLA) occurred in Rolwaling on April 19, 2020. Investigation revealed that the automated method incorrectly identified the boundaries between rocks and snow within high-elevation snowfields as the snowline. These protruding rock outcrops within snowfields differ from the snowline that manual operators would often identify; the lower boundary of the dominant snow cover. In our method, small polygons were removed to reduce the statistical relevance of these false positives; larger snow-free rock outcrops, however, are clearly prevalent in the Rolwaling domain. Even if such rock boundaries are not entirely removed, they generally have a small impact on the final SLA because they contribute relatively few grid points compared to the true snowline. In this particular scene, extensive cloud cover masked a large area, reducing the number of correctly identified snowline grid points (Fig. S5). In such cases, the influence of rock-snow boundaries is magnified, biasing the SLA towards higher elevations. The approach by Girona-Mata et al. (2019) involved masking elevations above a certain threshold to exclude ridgeline or rock outcrops snowlines. However, aiming for a method applicable globally, we did not apply a single, definitive threshold in this study. A potential solution is to exclude scenes where the number of unmasked snowline grid points is too low, considering the possibility of significant error impact. Due to those errors, our automated extraction method may be unsuitable for pinpointing the exact snowline on a specific day, especially under extensive cloud cover (introducing spatial bias based on the apparent snow boundaries). Nonetheless, it remains useful for analyzing long-term trends and seasonal patterns over large areas.~~

4.3. Reliability of trend detection

Our data-inclusive approach to snowline analyses mixes four satellite sensors with differing radiometric capabilities and sampling biases. The three Landsat sensors exhibit broad similarities in terms of spectral and temporal sampling, although with considerable improvements for Landsat 8, in particular (Paul et al, 2016). Collectively, these three sensors led to a relatively stable temporal sampling over our five study catchments, but the inclusion of Sentinel-2 data substantially increases the quantity of observations for the later period (Fig. S3-S7), in addition to the slightly different sensor characteristics. We therefore tested the effect of the Sentinel-2 data inclusion on our trend retrieval approach. The retrieved SLA trends differ for each site (up to 2.6 m

yr^{-1} difference) depending on the inclusion of Sentinel-2 data, but at no site does the trend direction or significance change based on this dataset (Fig. S14-S18).

All four sensors exhibited a similar seasonal sampling (Fig. S11), and the inclusion of Sentinel-2 data had minimal effect on the seasonal harmonic regression of SLA (Fig. S19-S23). However, all four sensors exhibited reduced sampling during the monsoon months due to the extensive summer cloud cover, so evaluate the reliability of the trend retrieval for reduced data sampling through a synthetic trend retrieval experiment. Beginning with a sampled harmonic and a random trend similar to that measured at our sites, we introduce noise and reduced monsoon image availability (Fig. S24-28). Our experiment highlights that the seasonal decomposition approach is robust to both noise and seasonal sampling biases, and successfully retrieves the imposed trends to within 2.5 m yr^{-1}. Our results highlight that standard regressions of oscillations around trends, even without sampling errors and biases, are subject to produce erroneous trends due to edge effects. This emphasizes the importance of long records and careful trend retrieval, such as with our seasonal decomposition approach, for environmental records with strong variability.

4.4 Limitations, advantages, and future perspectives

A major limitation for our study is the inconsistent data availability over time due to changing sensor missions, cloud cover, and varying extent of observations. Image availability is improving due to the increased number of operational imagers, but could have a strong impact on both the characterization of seasonal snow dynamics, especially for earlier periods, as well as the robust detection of a trend. A second major limitation is the prevalence of cloud cover, which further limits the usable area of affected images, and can, in some cases, lead to biases in the detected snowline due to undersampling. This can be mitigated with more stringent cloud coverage criteria, but will further reduce image availability for severely cloud-affected regions. Our cloud masking was largely successful for the evaluation scenes, but is likely to fail in some situations, leading to false snowline detections. As detailed above, our method is able to successfully recover snowlines and snowline trends despite these challenges.

The combination of multiple datasets with differing footprints, compounded by variable cloud cover and deep shadows, can lead sequential scenes to differ in snowline, but this can be the result of spatial sampling biases. Although our evaluation of the automated snowline retrieval showed its high accuracy relative to manual datasets (Table 2), it is clear that sampling biases due to spatial coverage can lead to statistical differences at the catchment scale (Fig. S10). In our study, differences in spatial coverage may have increased the variability of derived catchment snowlines even over short timescales. Our results indicate SLA variations are typically 200m within 10-20 days based on a variable-lag sensor cross-comparison (Fig. S28). This is reflected in the spread of seasonal retrieved SLA values (Fig. 3) but should not affect our derived trends. Nevertheless the challenge of spatial sampling underlines the importance of complete spatial coverage for integrated snowline assessments, encouraging the use of future rapid-repeat and cloud-insensitive snow monitoring methods (e.g. Tsai et al., 2019). We note that an advantage of our methodology is its transferability, and additional snow cover data products could easily be included in the analysis. Our full approach is directly transferable to Landsat 9, launched in 2021, or other high-resolution satellites that will be launched soon, will allow for longer and more detailed analyses. In addition, our method can be applied to wider areas as it leverages cloud-accessible global datasets and cloud processing.

This study used top-of-atmosphere radiances from multiple sensors to determine snowcover based on a fixed NDSI threshold; this simple approach showed close correspondence with independent evaluation datasets, and the similar method of Girona-Mata et al. (2019) also produced reliable snow cover at the Langtang site. Future developments could, in the future, be applied to homogenized surface reflectances with a fractional snow cover algorithm (Rittger et al., 2021). Further adaptations to the method, to enable application more broadly, could include temporal stacking, data fusion, or a different statistical definition of the snowline, in order to further control for spatial sampling challenges. In addition, to reduce the effect of spectral differences between Landsat and Sentinel-2 sensors on our derived snowlines, future efforts could make use of recent harmonized products (e.g. Feng et al., 2024).

An advantage of our method leveraging high-resolution sensors, compared to ~~a~~the standard snowline detection method leveraging MODIS data (Krajci et al., 2014), is its high ~~sensitivity to~~ spatial precision, which enabled us to examine aspect differences in snowline and to resolve snow at high altitudes~~, which comes from the high resolution of utilized satellites. The coarse~~. The coarser spatial resolution of MODIS snow cover products (500m) results in a crude representation of steeper topography, which leads to a high snow cover dropout rate ~~for~~at high elevations (e.g., Colleen et al., 2018), causing the detected SLA to jump to very high elevations in ~~summertime easily. Therefore,~~summer. As a result, the SLAs obtained from MODIS ~~are~~were much higher than SLAs from our method at all sites during the monsoon season, as high-elevation snow ~~is~~was essentially undetected (Fig. S6). ~~On the other hand~~In contrast, the low-elevation discrepancies in SLAs ~~seem~~appear to occur mainly in Satopanth and occasionally in Hidden Valley (Fig. S6). Upon examining the snowlines in Satopanth, we discovered that many north-facing slopes ~~are in shadow due to the~~were shadowed by topography. As a result, our method, which masks shadows, tends to detect snowlines that are biased towards south-facing slopes. This likely explains the discrepancies observed at lower elevations in Satopanth, as ~~the~~ snowlines detected on higher south-facing slopes ~~are~~were not fully captured. One option to address this issue ~~would be~~is to apply a statistical correction, considering that we have measured the aspect difference and can identify which areas of the domain have been sampled versus those that have not. This correction would help ~~in providing~~provide a more accurate representation of the SLA across areas with various ~~topography~~topographies.

~~Another advantage of our methodology is its transferability. Although Landsat 5/7/8 and Sentinel-2 are selected in this study, additional satellite data can easily be added to the analysis if the data is stored in the Google Earth Engine. Using Landsat 9, launched in 2021, or other higher-resolution satellites that will be launched soon will allow for longer and more detailed analysis. In addition, our method can be readily applied to a wider area, as it automatically detects SLA through the e Google Earth Engine.~~

Our study demonstrated significant regional differences in snow cover dynamics across ~~the~~ five catchments in the Himalayas, ~~suggesting that various regions, such as arid areas or those where winter coincides with the rainy season, may each have unique~~ highlighting the diversity of snow ~~cover dynamics.~~phenology in similar climates and emphasising the need for further detailed investigations in distinct climates. By applying our automated method to broader areas, such as the whole of Asia or globally, ~~we could~~future studies can investigate the distinct characteristics of snow dynamics in different regions~~.~~; application to strongly differing domains will, however, need further evaluation. This approach will enable us to examine ~~the~~ changes in the SLA worldwide and identify the factors controlling ~~factors behind~~ these changes, contributing to a deeper knowledge of the spatial and temporal distributions of snow cover and the hydrology in the cryosphere and downstream regions. Future works on SLA detection ~~on~~at larger scales could provide process-based advances beyond the foundations achieved with coarse sensors such as MODIS.

~~6~~5 Conclusion

In this study, we demonstrate~~We propose~~ an algorithm to automatically detect the catchment snowline altitude (SLA) from multispectral remote sensing data and apply it to five ~~glaciated~~glacierized monsoonal catchments in the High Mountain Asia ~~(HMA)~~ region~~. The detected SLA from~~ for the 1999 ~~to~~ -2019 ~~reveals both regional consistencies~~period. Our results highlight strongly variable seasonal SLA amplitudes between the five sites. All sites exhibit maximum SLA values during the monsoon of 5500 m a.s.l., with the exception of the topographically-limited Parlung catchment, as well as minimum values during the winter, when the scatter of SLA is also very high. This behaviour and ~~differences across the target~~the variable aspect dependence during these periods highlight the contrast between temperature control on SLA, during the monsoon, and precipitation control during the winter. Our results indicate rising SLA at three of the study catchments~~. The monthly time series of SLA indicated that the long-term trend of SLA varies from −15.6 m yr^{-1}~~ (Hidden Valley, Langtang, and Rolwaling) with trends up to +14.4 m yr^{-1}~~: increasing in the three catchments in the Nepalese Himalaya, decreasing in~~, no statistical trend at the Parlung catchment, and a lowering SLA at Satopanth ~~in the western Indian Himalaya, and showing no statistically significant~~(−15.6 m yr^{-1}). Decadal changes in ~~Parlung in southeastern Tibet. The analysis of decadal changes in~~the monthly SLA and climatic factors suggests that ~~the~~ long-term SLA trends ~~in SLA~~ are primarily controlled by the balance between higher temperatures during the monsoon and lower temperatures with increased snowfall during winter. ~~While time-series changes are strongly influenced by meteorological factors, seasonal patterns depend on topographical features in addition to meteorological factors.~~ Further application of our method ~~to~~on a broader scale could provide novel insights into the ~~spatio-temporal~~spatiotemporal variation ~~of~~in snow cover and its controlling factors~~.~~, and providing control for numerical modelling efforts. This ~~would~~will contribute to a deeper understanding of the future state of snow cover and related hydrology, which ~~is~~are crucial for water resource management and climate change adaptation ~~efforts~~.

Formatted: Font: Times New Roman

Formatted: Font: Times New Roman

Formatted: Indent: First line: 0"

Formatted: Font: Times New Roman

Formatted: Font: Times New Roman

Formatted: Font: Times New Roman

Formatted: Font: Times New Roman

Formatted: Font: Times New Roman

Formatted: Font: Times New Roman

Formatted: Font: Times New Roman

Code availability

The script for automatic detection of SLA is available through ~~the~~ GitHub ~~site.~~.upon request: https://github.com/miles916/GEE_SLATools

Data availability

HydroSHEDS data, Landsat 5/7/8 data, Sentinel-2 data and AW3D30 are available through the Earth Engine Data Catalog (~~https://developers.google.com/earth-engine/datasets/catalog/landsat)~~https://developers.google.com/earth-engine/datasets/catalog/) which is a data catalogue of the Google Earth Engine that is a cloud-based geospatial analysis platform. The latest version of the GAMDAM Inventory data~~,~~ used in this ~~article, is~~study are available on the PANGAEA ~~site~~website (https://doi.org/10.1594/PANGAEA.891423). Outline data ~~of~~for the supraglacial debris ~~is~~are available ~~from~~in the supplemental data of Scherler et al. (2018). ~~The surface~~Surface water body data ~~is~~are available ~~through~~from the official ~~website of~~ Global Surface Water website (https://global-surface-water.appspot.com/~~,~~; Pekel et al., 2016). RapidEye and PlanetScope data are available ~~through~~from the European Space Agency (https://earth.esa.int/eogateway/missions/rapideye~~,~~ and

Formatted: Font color: Blue

https://earth.esa.int/eogateway/missions/planetscope). Finally, meteorological data from ERA5 ~~are~~were available via the Copernicus Climate Data Store (https://doi.org/10.24381/cds.adbb2d47~~,~~; Hersbach et al., 2023).

Author contributions

ESM, FP, and KF ~~design~~designed the study. OS developed the automated algorithm and ~~wrote~~prepared the manuscript. OS analysed the data with the support of KF and AS. KF and AS ~~conducted the manual delineation of~~ manually delineated snowlines for validation. All authors discussed the analysis and results and contributed to the ~~paper~~ writing of the paper.

Competing interests

The authors declare that they have no conflict of interest.

Acknowledgments

We thank Maud Bernat for helping with the modification of the automatic detection code, and Michael McCarthy for preparing snowline data derived from the MODIS satellite.

Financial support

This research ~~has been~~was supported by the JSPS-SNSF (Japan Society for the Promotion of Science and Swiss National Science Foundation) Bilateral Programmes project (HOPE, High-elevation precipitation in High Mountain Asia; JPJSJRP 20191503 / Grant 183633), and JSPS KAKENHI (Grant Number 23K13417 and 23H01509).

References

Bao, Y. and You, Q.: How do westerly jet streams regulate the winter snow depth over the Tibetan Plateau?, Clim. Dyn., 53, 353–370, https://doi.org/10.1007/s00382-018-4589-1, 2019.

Buri, P., Fatichi, S., Shaw, T. E., Fyffe, C. L., Miles, E. S., McCarthy, M. J., Kneib, M., Ren, S., Jouberton, A., Fugger, S., Jia, L., Zhang, J., Shen, C., Zheng, C., Menenti, M., & Pellicciotti, F. Land surface modeling informed by earth observation data: Toward understanding blue–green–white water fluxes in High Mountain Asia. Geo-Spatial Information Science, 27(3), 703–727. https://doi.org/10.1080/10095020.2024.2330546, 2024.

Buri, P., Fatichi, S., Shaw, T. E., Miles, E. S., McCarthy, M. J., Fyffe, C. L., Fugger, S., Ren, S., Kneib, M., Jouberton, A., Steiner, J., Fujita, K., & Pellicciotti, F. Land Surface Modeling in the Himalayas: On the Importance of Evaporative Fluxes for the Water

Balance of a High-Elevation Catchment. Water Resources Research, 59(10), e2022WR033841. https://doi.org/10.1029/2022WR033841, 2023.

Burns, P., & Nolin, A. Using atmospherically-corrected Landsat imagery to measure glacier area change in the Cordillera Blanca, Peru from 1987 to 2010. Remote Sensing of Environment, 140, 165–178. https://doi.org/10.1016/j.rse.2013.08.026, 2014.

Cannon, F., Carvalho, L.M.V., Jones, C., and Bookhagen, B.: Multi-annual variations in winter westerly disturbance activity affecting the Himalaya. Clim. Dyn., 44, 441–455, https://doi.org/10.1007/s00382-014-2248-8, 2015.

Cleveland, R. B., Cleveland, W. S., McRae, J. E., & Terpenning, I. STL: A Seasonal-Trend Decomposition Procedure Based on Loess. Journal of Official Statistics, 6, 3-33, 1990.

~~Mortimer, C. A. and Sharp, M.: Spatiotemporal variability of Canadian High Arctic glacier surface albedo from MODIS data, 2001–2016, The Cryosphere, 12, 701–720, https://doi.org/10.5194/tc-12-701-2018, 2018.~~

Deng, G., Tang, Z., Hu, G., Wang, J., Sang, G., and Li, J.: Spatiotemporal Dynamics of Snowline Altitude and Their Responses to Climate Change in the Tienshan Mountains, Central Asia, during 2001–2019, Sustainability, 13(7), 3992, https://doi.org/10.3390/su13073992, 2021.

Dozier, J. Spectral signature of alpine snow cover from the landsat thematic mapper. Remote Sensing of Environment, *28*, 9–22. https://doi.org/10.1016/0034-4257(89)90101-6, 1989.

Feng, S., Cook, J. M., Onuma, Y., Naegeli, K., Tan, W., Anesio, A. M., Benning, L. G., & Tranter, M. Remote sensing of ice albedo using harmonized Landsat and Sentinel 2 datasets: Validation. International Journal of Remote Sensing, 45(19–20), 7724–7752. https://doi.org/10.1080/01431161.2023.2291000, 2024.

Gascoin, S., Grizonnet, M., Bouchet, M., Salgues, G., & Hagolle, O. Theia Snow collection: High-resolution operational snow cover maps from Sentinel-2 and Landsat-8 data. Earth System Science Data, 11(2), 493–514. https://doi.org/10.5194/essd-11-493-2019 , 2019.

Girona-Mata, M., Miles, E. S., Ragettli, S., and Pellicciotti, F.: High-resolution snowline delineation from Landsat imagery to infer snow cover controls in a Himalayan catchment, Water Resour. Res., 55, 6754–6772, https://doi.org/10.1029/2019WR024935, 2019.

Härer, S., Bernhardt, M., Siebers, M., & Schulz, K. On the need for a time- and location-dependent estimation of the NDSI threshold value for reducing existing uncertainties in snow cover maps at different scales. The Cryosphere, 12(5), 1629–1642. https://doi.org/10.5194/tc-12-1629-2018, 2018.

Hersbach, H., Bell, B., Berrisford, P., Hirahara, S., Horányi, A., Muñoz-Sabater, J., Nicolas, J., Peubey, C., Radu, R., Schepers, D., Simmons, A., Soci, C., Abdalla, S., Abellan, X., Balsamo, G., Bechtold, P., Biavati, G., Bidlot, J., Bonavita, M., De Chiara, G., Dahlgren, P., Dee, D., Diamantakis, M., Dragani, R., Flemming, J., Forbes, R., Fuentes, M., Geer, A., Haimberger, L., Healy, S., Hogan, R. J., Hólm, E., Janisková, M., Keeley, S., Laloyaux, P., Lopez, P., Lupu, C., Radnoti, G., Rosnay, P., Rozum, I., Vamborg, F., Villaume, S., and Thépaut, J.: The ERA5 global reanalysis, Q J R Meteorol. Soc., 146, 1999–2049, https://doi.org/10.1002/qj.3803, 2020.

Immerzeel, W. W., Lutz, A. F., Andrade, M., Bahl, A., Biemans, H., Bolch, T., Hyde, S., Brumby, S., Davies, B. J., Elmore, A. C., Emmer, A., Feng, M., Fernández, A., Haritashya, U., Kargel, J. S., Koppes, M., Kraaijenbrink, P. D. A., Kulkarni, A. V., and Maye, J. E. M.: Importance and vulnerability of the world's water towers, Nature, 577, 364–369, https://doi.org/10.1038/s41586-019-1822-y, 2020.

Kraaijenbrink, P. D. A., Stigter, E. E., Yao, T., and Immerzeel, W. W.: Climate change decisive for Asia’s snow meltwater supply, Nat. Clim. Chang, 11, 591–597, https://doi.org/10.1038/s41558-021-01074-x, 2021.

Krajčí, P., Holko, L., Perdigao, R. A. P., and Parajka, J.: Estimation of regional snowline elevation (RSLE) from MODIS images for seasonally snow covered mountain basins, J. Hydrol., 519(PB), 1769–1778, https://doi.org/10.1016/j.jhydrol.2014.08.064, 2014.

Krishnan, R., Sabin, T. P., Madhura, R. K. et al.: Non-monsoonal precipitation response over the Western Himalayas to climate change, Clim. Dyn., 52, 4091–4109, https://doi.org/10.1007/s00382-018-4357-2, 2019.

Johnston, J., Jacobs, J. M., & Cho, E. Global Snow Seasonality Regimes from Satellite Records of Snow Cover. https://doi.org/10.1175/JHM-D-23-0047.1, 2023.

Lehner, B., and Grill, G.: Global river hydrography and network routing: baseline data and new approaches to study the world's large river systems. Hydrol. Process., 27, 2171-2186. https://doi.org/10.1002/hyp.9740, 2013.

Lievens, H., Demuzere, M., Marshall, H. P., Reichle, R. H., Brucker, L., Brangers, I., Rosnay, P., Dumont, M., Girotto, M., Immerzeel, W. W., Jonas, T., Kim, E. J., Koch, I., Marty, C., Saloranta, T., Schöber, J., and De Lannoy, G. J. M.: Snow depth variability in the Northern Hemisphere mountains observed from space, Nat. Commun., 10, 4629, https://doi.org/10.1038/s41467-019-12566-y, 2019.

Liu, Y., Fang, Y., & Margulis, S. A. Spatiotemporal distribution of seasonal snow water equivalent in High Mountain Asia from an 18-year Landsat–MODIS era snow reanalysis dataset. The Cryosphere, 15(11), 5261–5280. https://doi.org/10.5194/tc-15-5261-2021, 2021.

Maussion, F., Scherer, D., Mölg, T., Collier, E., Curio, J., & Finkelnburg, R. Precipitation Seasonality and Variability over the Tibetan Plateau as Resolved by the High Asia Reanalysis*. Journal of Climate, 27(5), 1910–1927. https://doi.org/10.1175/JCLI-D-13-00282.1, 2014.

McFadden, E. M., Ramage, J., and Rodbell, D. T.: Landsat TM and ETM+ derived snowline altitudes in the Cordillera Huayhuash and Cordillera Raura, Peru, 1986–2005, The Cryosphere, 5, 419–430, https://doi.org/10.5194/tc-5-419-2011, 2011.

Mernild, S. H., Pelto, M., Malmros, J. K., Yde, J. C., Knudsen, N. T., & Hanna, E. Identification of snow ablation rate, ELA, AAR and net mass balance using transient snowline variations on two Arctic glaciers. Journal of Glaciology, 59(216), 649–659. https://doi.org/10.3189/2013JoG12J221, 2013.

Morinaga, Y. Seasonal variation of snowline in Langtang Valley, Nepal Himalayas, 1985–1986. Bulletin of glacier research, 5, 49, 1987.

Formatted: Font color: Auto

Mortimer, C. A. and Sharp, M.: Spatiotemporal variability of Canadian High Arctic glacier surface albedo from MODIS data, 2001–2016, The Cryosphere, 12, 701–720, https://doi.org/10.5194/tc-12-701-2018, 2018.

Muhammad, S., & Thapa, A. An improved Terra–Aqua MODIS snow cover and Randolph Glacier Inventory 6.0 combined product (MOYDGL06*) for high-mountain Asia between 2002 and 2018. Earth System Science Data, 12(1), 345–356. https://doi.org/10.5194/essd-12-345-2020, 2020.

Notarnicola, C. Overall negative trends for snow cover extent and duration in global mountain regions over 1982–2020. Scientific Reports, 12(1), 13731. https://doi.org/10.1038/s41598-022-16743-w, 2022.

Nuimura, T., Sakai, A., Taniguchi, K., Nagai, H., Lamsal, D., Tsutaki, S., Kozawa, A., Hoshina, Y., Takenaka, S., Omiya, S., Tsunematsu, K., Tshering, P., and Fujita, K.: The GAMDAM glacier inventory: a quality-controlled inventory of Asian glaciers, The Cryosphere, 9, 849–864, https://doi.org/10.5194/tc-9-849-2015, 2015.

Palazzi, E., Mortarini, L., Terzago, S., and Hardenberg, J.: Elevation-dependent warming in global climate model simulations at high spatial resolution, Clim. Dyn., 52, 2685–2702, https://doi.org/10.1007/s00382-018-4287-z, 2019.

Paul, F., Winsvold, S. H., Kääb, A., Nagler, T., & Schwaizer, G. Glacier Remote Sensing Using Sentinel-2. Part II: Mapping Glacier Extents and Surface Facies, and Comparison to Landsat 8. Remote Sensing, 8(7), Article 7. https://doi.org/10.3390/rs8070575, 2016.

Pekel, J. F., Cottam, A., Gorelick, N., and Belward, A. S.: High-resolution mapping of global surface water and its long-term changes, Nature, 540, 418–422, https://doi.org/10.1038/nature20584, 2016.

Pellicciotti, F., Raschle, T., Huerlimann, T., Carenzo, M., and Burlando, P.: Transmission of solar radiation through clouds on melting glaciers: a comparison of parameterizations and their impact on melt modelling, J. Glaciol., 57(202), 367-381, https://doi.org/10.3189/002214311796406013, 2011.

Pritchard, H.D.: Asia's shrinking glaciers protect large populations from drought stress, Nature, 569, 649–654, https://doi.org/10.1038/s41586-019-1240-1, 2019.

Racoviteanu, A. E., Rittger, K., and Armstrong, R.: An Automated Approach for Estimating Snowline Altitudes in the Karakoram and Eastern Himalaya From Remote Sensing, Front. Earth Sci., 7, 220, https://doi.org/10.3389/feart.2019.00220, 2019.

Roessler, S., & Dietz, A. J. Development of Global Snow Cover—Trends from 23 Years of Global SnowPack. Earth, 4(1), Article 1. https://doi.org/10.3390/earth4010001, 2023.

Rittgerm, K., Bormann, K. J., Bair, E. H., Dozier, J., and Painter, T. H.: Evaluation of VIIRS and MODIS Snow Cover Fraction in High-Mountain Asia Using Landsat 8 OLI, Front. Remote Sens., 2, 647154, https://doi.org/10.3389/frsen.2021.647154, 2021.

Sakai, A.: Brief communication: Updated GAMDAM glacier inventory over high-mountain Asia, The Cryosphere, 13, 2043–2049, https://doi.org/10.5194/tc-13-2043-2019, 2019.

Scherler, D., Wulf, H., and Gorelick, N.: Global assessment of supraglacial debris-cover extents, Geophys. Res. Lett., 45, 11798–11805, https://doi.org/10.1029/2018GL080158, 2018.

Smith, T. and Bookhagen, B.: Changes in seasonal snow water equivalent distribution in High Mountain Asia (1987 to 2009), Sci. Adv., 4, e1701550, https://doi.org/10.1126/sciadv.1701550, 2018.

Spiess, M., Huintjes, E., and Schneider, C.: Comparison of modelled- and remote sensing- derived daily snow line altitudes at Ulugh Muztagh, northern Tibetan Plateau, J. Mt. Sci., 13, 593–613, https://doi.org/10.1007/s11629-015-3818-x, 2016.

Stigter, E. E., Wanders, N., Saloranta, T. M., Shea, J. M., Bierkens, M. F. P., and Immerzeel, W. W.: Assimilation of snow cover and snow depth into a snow model to estimate snow water equivalent and snowmelt runoff in a Himalayan catchment, The Cryosphere, 11, 1647–1664, https://doi.org/10.5194/tc-11-1647-2017, 2017.

Stillinger, T., Roberts, D. A., Collar, N. M., and Dozier, J.: Cloud masking for Landsat 8 and MODIS Terra over snow-covered terrain: Error analysis and spectral similarity between snow and cloud, Water Resour. Res., 55, 6169–6184. https://doi.org/10.1029/2019WR024932, 2019.

Takaku, J., Tadono, T., Tsutsui, K., and Ichikawa, M.: Quality Improvements of 'AW3D' Global Dsm Derived from Alos Prism, IGARSS 2018 - 2018 IEEE International Geoscience and Remote Sensing Symposium, 1612-1615, https://doi.org.10.1109/IGARSS.2017.8128293, 2018.

Tang, Z., Wang, X., Deng, G., Wang, X., Jiang, Z., and Sang, G.: Spatiotemporal variation of snowline altitude at the end of melting season across High Mountain Asia, using MODIS snow cover product, Adv. Space Res., 66, 2629–2645, https://doi.org/10.1016/j.jhydrol.2022.128438, 2020.

Tang, Z., Deng, G., Hu, G., Zhang, H., Pan, H., & Sang, G. Satellite observed spatiotemporal variability of snow cover and snow phenology over high mountain Asia from 2002 to 2021. Journal of Hydrology, 613, 128438. https://doi.org/10.1016/j.jhydrol.2022.128438, 2022.

Tsai, Y.-L. S., Dietz, A., Oppelt, N., & Kuenzer, C. Wet and Dry Snow Detection Using Sentinel-1 SAR Data for Mountainous Areas with a Machine Learning Technique. Remote Sensing, 11(8), 895. https://doi.org/10.3390/rs11080895, 2019.

Viviroli, D., Kummu, M., Meybeck, M., Kallio, M., and Wada, Y.: Increasing dependence of lowland populations on mountain water resources, Nat. Sustain., 3, 917–928, https://doi.org/10.1038/s41893-020-0559-9, 2020.

Yang, W., Yao, T. D., Guo, X. F., Zhu, M. L., Li, S. H., and Kattel, D. B.: Mass balance of a maritime glacier on the southeast Tibetan Plateau and its climatic sensitivity, J. Geophys. Res.-Atmos., 118, 9579–9594, https://doi.org/10.1002/jgrd.50760, 2013.